IET Journals
The Institution of Engineering and Technology

A Decomposition Strategy for Inertia-Aware Microgrid Planning Models

ISSN 1751-8644
doi: 0000000000
www.ietdl.org

Agnes Marjorie Nakiganda[1], *Shahab Dehghan*[2], *Petros Aristidou*[3]

[1] *Department of Electrical Engineering and Electronic Engineering, Imperial College London, United Kingdom*
[2] *School of Engineering, Newcastle University, United Kingdom*
[3] *Department of Electrical Engineering and Computer Engineering and Informatics, Cyprus University of Technology, Cyprus*
** E-mail: a.nakiganda@imperial.ac.uk*

Abstract: The growing penetration of converter-Interfaced Generators (CIG) in electricity grids has diminished inertia levels. Micro-Grids (MGs), with their high penetration of CIGs, are particularly vulnerable to the reduced inertia levels presenting a challenge to their secure and reliable operation. MG system planning must now incorporate the analysis of dynamic system security complementing traditional resource adequacy assessments. However, integrating transient security constraints into MG planning is complex due to the non-convex and non-linear nature of the analytical expressions for frequency metrics and power flow constraints. To address this challenge, this paper presents a decomposition-based approach to the MG investment planning problem that leverages dual solutions to derive dual-cutting planes, effectively constraining the feasible solution space. This enhances computational tractability and optimality by ensuring that the sensitivity of decisions at each stage can be accurately captured. This facilitates the identification of cost-effective investment strategies that balance economic objectives and security requirements, optimizing the placement of inertia services and accelerating algorithm convergence. The significance of the proposed algorithms is validated on a low- and medium-voltage network under various operating scenarios and security levels. Results demonstrate that the proposed algorithms yield solutions that are more sensitive to frequency support needs and converge more rapidly.

Nomenclature

Functions

$\Theta^{\mathrm{gm,opr}}$	Total operational costs in the grid-connected mode [\$].
$\Theta^{\mathrm{im,opr}}_{to}$	Total penalty costs of disconnecting loads from MG at hour t in representative day o in the islanded mode [\$].
$\breve{\Theta}^{\mathrm{im,opr}}$	Vector-valued function of total penalty costs of disconnecting loads from MG in the islanded mode [\$].
Θ^{inv}	Total investment costs [\$].

Indices

g	Index of generators, $g \in \{c, d, s, v\}$.
i	Index of nodes, i^+/i^- being the node before/after node i.
l	Index of lines, l^{i^+}/l^{i^-} being the line connecting upstream or downstream of node i.
o	Index of representative days.
t	Index of hours.
ψ	Index of iterations.

Parameters

c_g	Marginal cost of generator g [\$/kWh].
c^{inv}_g	Annualised investment cost of generator g [\$].
c^{curt}_i	Penalty cost of curtailing demand at node i [\$/kWh].
c^{flx}_i	Penalty cost of shifting demand at node i [\$/kWh].
c^{inv}_l	Annualised investment/reinforcement cost of line l [\$].
$c^{\mathrm{b/s}}_{to}$	Buying/selling price of electricity from/to the main grid at hour t in representative day o [\$/kWh].
D	Normalised damping constant of all generators [p.u.].
D_g	Damping constant of Synchronous Generator (SG) g, D_s is the weighted average of all SGs [p.u.].
D_v	Virtual damping constant of Virtual Synchronous Machine (VSM) based Converter-Interfaced Generator (CIG) v, D_c is the weighted average of all CIGs [p.u.].
$d^{\mathrm{pc/qc}}_{ito}$	Constant part of active/reactive power demand at node i, hour t, and representative day o [kW/kVAr].
e_{io}	Flexible energy demand at node i and representative day o [kWh].
F_g	Fraction of the total power generated by the turbine of SG g, F_s being the weighted average of all SGs [p.u.].
K_d	Power gain factor of droop-based CIG d [p.u.].
K_g	Mechanical power gain factor of SG g [p.u.].
M	Normalised inertia constant of all generators [s].
M_g	Inertia constant of SG g, M_s is the normalised inertia constant of all SGs [s].
M_v	Virtual inertia constant of CIG v with VSM control, M_c is the normalised inertia of all CIGs [s].
p^{av}_{gto}	Maximum available power for generator g at hour t and representative day o [kW].
p^{nom}_g	Nominal capacity of generator g [kW].
p^{res}_g	Minimum reserve power capacity for transient frequency response of generator g [kW].
R_d	Droop of CIG d with droop control, R_c being the weighted average of all CIGs [%].
R_g	Droop of SG g, R_s being the weighted average of all SGs [%].
$r^{\mathrm{dn/up}}_g$	Ramp-down/ramp-up limit of generator g [kW/h].
$r_{l^{i-}}$	Resistance of the line l connecting nodes (i, i^-) [Ω].
$\overline{S}_{l^{i-}}$	Capacity of line l connecting nodes (i, i^-) [kVA].
$T_{d/v}$	Time constant of CIG with droop/VSM control [s].
T_g	Turbine time constant of SG g [s].
$x_{l^{i-}}$	Reactance of line l connecting nodes (i, i^-) [Ω].
$z^0_{l^{i-}}$	Initial status of line l connecting nodes (i, i^-) (i.e., 1/0: built/not-built).
ζ	Damping ratio.
ω_n	Natural frequency [Hz].
τ_o	Weighting factor of representative day o.

Sets

$\mathcal{C}$	Set of CIGs, $\mathcal{C}^i$ being the set of generators connected to node i.
$\mathcal{C}^{d/v}$	Set of CIGs with droop/VSM control scheme.
$\mathcal{L}$	Set of lines connecting neighboring nodes.
$\mathcal{N}$	Set of nodes, $\mathcal{N}^i$ being the set of nodes after and connected to node i.
$\mathcal{O}$	Set of representative days.
$\mathcal{S}$	Set of SGs, $\mathcal{S}^i$ being the set of generators connected to node i.

$\mathcal{T}$ Set of hours in a representative day.
$\Phi^{\mathrm{fr,opr}}$ Feasible space of frequency support-related variables.
$\Phi^{\mathrm{gm,opr}}$ Feasible space of operational variables in grid-connected mode.
$\Phi^{\mathrm{im,opr}}$ Feasible space of operational variables in islanded mode.

Symbols

$\hat{\bullet}/\check{\bullet}$ Upward/downward deviation of the quantity $\bullet$ in the islanded mode from its value in the grid-connected mode.
$|\bullet|$ Cardinality of the set $\bullet$.
$\underline{\bullet}/\overline{\bullet}$ Lower/upper bounds of the quantity $\bullet$.

Variables

$d^{\mathrm{p/q}}_{ito}$ Active/reactive power demand at node i, hour t, and representative day o $[\mathrm{kW/kVAr}]$.
$d^{\mathrm{pf/qf}}_{ito}$ Flexible part of active/reactive power demand at node i, hour t, and representative day o $[\mathrm{kW/kVAr}]$.
$f_{l^{i^{+/-}}to}$ Square of current magnitude flowing into line $l^{i^{+/-}}$ at hour t and representative day o $[A^2]$
$P_{l^{i^{+/-}}to}$ Active power flow of a line connecting nodes $(i, i^{+/-})$ at hour t and representative day o $[\mathrm{kW}]$.
p/q_{gto} Active/reactive power generation of generator g at hour t and representative day o $[\mathrm{kW/kVAr}]$.
$p/q^{\mathrm{b/s}}_{to}$ Active/reactive power bought/sold from/to the main grid at hour t and representative day o $[\mathrm{kW/kVAr}]$.
$Q_{l^{i^{+/-}}to}$ Reactive power flow of a line connecting nodes $(i, i^{+/-})$ at hour t and representative day o $[\mathrm{kVAr}]$.
v_{ito} Voltage magnitude at node i, hour t, and representative day o $[V]$.
z_g Binary variable indicating the investment status of generator g (i.e., $1/0$: built/not-built).
$z^{\mathrm{im,pc}}_{ito}$ Binary variable indicating the connection status of power demand at node i, hour t, and representative day o in the islanded mode (i.e., $1/0$: connected/disconnected).
z_l Binary variable indicating the investment/reinforcement status of line l.
$z^{\mathrm{gm,p/q}}_{to}$ Binary variable preventing simultaneous import and export of active/reactive power at hour t and representative day o.

Vectors

$\boldsymbol{\chi}$ Vector of all investment and operational variables.
$\boldsymbol{\chi}^{\mathrm{gm,opr}}$ Vector of operational variables in grid-connected mode.
$\boldsymbol{\chi}^{\mathrm{im,opr}}$ Vector of operational variables in islanded mode.
$\boldsymbol{\chi}^{\mathrm{inv}}$ Vector of investment variables.

1 Introduction

The ability to operate in dual modes (i.e., connected to the grid or disconnected from the grid as autonomous islands) has cemented Micro-Grids (MGs) as pivotal infrastructure to increase the resilience of the grid. In other words, MGs are capable of enhancing the resilience of the system by forming autonomous islands during extreme events in the grid, and consequently, ensuring the continuity of the power supply [1–3]. However, this is possible only if security is ensured *before*, *during*, and *after* MG islanding events.

An MG, is defined as "*a group of interconnected loads and distributed energy resources with clearly defined electrical boundaries that acts as a single controllable entity with respect to the grid and can connect and disconnect from the grid to enable it to operate in both grid-connected or island modes*" [4].

Decreased system inertia, exacerbated by the increasing penetration of Converter-Interfaced Generators (CIGs), can lead to significant frequency excursions during grid disturbances further affecting the survivability of an MG in post-islanded mode [5–8]. To enhance system survivability, various grid-supporting capabilities of CIGs can be exploited. However, to guarantee the availability of required levels of frequency support, a holistic approach to system planning is necessitated where not only resource adequacy is considered but also dynamic security constraints (i.e., relating to frequency evolution for various levels of disruption) are incorporated. This approach enables a comprehensive evaluation of each investment candidate, considering both their energy or power capacity and their potential contribution to frequency support for the system. System planning with inherent security evaluation of both *pre-* and *post-islanding* operating points of the MG, as well as the system trajectory during the transition to an island, ensures that operation is within acceptable limits and further ensures system preparedness for various events.

While steady-state security has been widely studied in MG planning problems using the power flow model and associated static constraints [9–12], dynamic security requires the inclusion of the system transient evolution model. The latter is usually represented by Differential Algebraic Equations (DAEs) and associated time-domain trajectory constraints defined by Grid Code regulations. However, adding dynamic security constraints in MG planning problems results in a highly complex optimisation problem, which cannot be easily solved by off-the-shelf optimisation packages.

A more tractable alternative strategy to evaluate dynamic security is with the use of analytically derived expressions for transient frequency evolution [13–15], that can be embedded into MG planning problems as proxies for trajectories of DAEs to assess different metrics ensuring the security of the system. These security metrics consist of frequency nadir, frequency zenith, Rate-of-Change of Frequency (RoCoF), and the steady-state post-transient frequency deviation. Note that these analytical expressions map the "control parameters" (i.e., system inertia, damping, and droop levels) to "system states" essential during frequency support. Although including analytical expressions in MG planning problems to evaluate the transient frequency evolution is more tractable than including DAEs, their highly non-linear characteristics result in a complicated optimisation problem.

The time-domain trajectory of the system frequency deviation has been described by a first-order ordinary differential equation in [14]. This dynamic model has been adopted in [16] to derive expressions for the frequency nadir, RoCoF, and quasi-steady-state frequency imposed on a stochastic scheduling problem. While the RoCoF and quasi-steady-state constraints are convex, the non-linear frequency nadir expression in [15] has been approximated by a bi-linear constraint with further sufficient conditions on the approximation defined by mixed-integer linear constraints. In [17], a two-step linearisation technique defined by an inner approximation utilising overestimating planes and the standard big-M technique has been introduced to linearise the nadir expression. Furthermore, the work in [18] has transformed the frequency nadir constraints into the capacity reserve constraints using a series of linear frequency security margin constraints formulated by piece-wise linearisation fitting of the non-linear expression. Additionally, the work in [19] has utilised ex-ante bound extractions on the variables of the nadir expression using potential dispatch conditions that have then been imposed in the security-constrained unit commitment problem replacing the non-linear nadir expression. References [20–22] have adopted a linearised approximation of the frequency nadir constraint. Moreover, data-driven methods based on neural networks and the support vector machine have been applied in [23] and [24], respectively, to approximate the frequency nadir expression.

The aforementioned studies have certain inaccuracies emanating from the adoption of simplified dynamic models, approximations of the frequency nadir constraint, or ex-ante limit extractions to simplify the planning model. Moreover, the characteristic properties of MGs have not been included in these studies. Due to the inaccuracy inherited from different approximations, a three-stage iterative algorithm with a sequential linearisation and bounds-tightening has been proposed in [25] using the more accurate low-order frequency model in [15]. The first stage of the problem ensures the optimality of the planning solution, while the second stage is a feasibility checking problem against the transient security problem. In the third stage, tighter bounds for power exchange with the main grid are formulated and generated for the first stage problem if infeasibilities exist in the second stage. Although the three-stage algorithm in [25] does not require any approximation of transient frequency constraints when applied to the optimisation problem, it finds a rather conservative solution. Additionally and more importantly, similar to the previous literature, the techno-economic effect of different generator parameters on the planning solution and frequency security limits has not been adequately studied in [25].

Motivated by the challenges mentioned above, two efficient multi-level decomposition strategies, utilising dual cutting planes based on the notion of Benders decomposition, are introduced in this paper to more cost-effectively solve the model presented in [25]. The dual cutting planes in the proposed decomposition strategies ensure that the techno-economic effects of the MG's parameter changes in the *feasibility-checking* problem are cost-effectively captured by the *investment and operational planning* problem. The proposed approach, therefore, allows for the decoupling of frequency services where emphasis can be applied to single or multiple services provision. This ensures optimal determination and provision of frequency services in MGs. Accordingly, the main contributions of this paper are threefold:

- A security-constrained MG investment planning solution that ensures sufficiency during pre- and post-islanding as well as transient security in the transitional period for unintended islanding scenarios.
- Two multi-level decomposition strategies are proposed to ensure tractable incorporation of non-linear transient frequency security constraints in the MG investment and operational planning problem. The proposed decomposition strategies utilise dual cutting planes to capture the effect of decisions made in the feasibility-checking sub-problems on decisions made in the investment and operational planning master problem. Subsequently, this enables the segmentation of different frequency services that can be provided by each generator or the system as a whole.
- To linearise the non-linear frequency nadir constraint, a first-order Taylor expansion is adopted in this paper. Note that higher orders can be utilised to enhance the accuracy of the solution at the expense of significantly higher computational time.

The remainder of this paper is organised as follows. Section 2 presents the formulation of the MG investment and operational planning model considering pre- and post-islanding constraints with only steady-state security constraints. In Section 3 the model is enhanced to include non-linear inertia and frequency security constraints associated with the transition to an islanded mode of operation. Section 4 describes the proposed decomposition strategies for the inertia-aware planning problem. Then, the case study results are presented in Section 5. Finally, the main conclusions are drawn in Section 6.

2 Microgrid Planning with Static Security Constraints

The proposed investment and operational planning model considers the effect of investment decisions on the operation of the MG in both grid-connected and islanded modes. Here, only the steady-state security constraints for post-islanded operation are included in the MG investment planning model. In the proposed model, uncertain variations of load demands and renewable generations during the planning horizon are characterized by a sufficient number of representative days, obtained by utilizing the k-means clustering technique [26]. Also, it is assumed islanding from the main grid may occur at each hour (indexed by $t \in \mathcal{T}$) of every representative day (indexed by $o \in \mathcal{O}$) to ensure the robustness of the optimal investment and operational plan against the worst-case unscheduled event in MG. The MG planning model with static islanding constraints can be compactly presented as follows:

$$\min_{\forall \boldsymbol{\chi}} \Theta^{\mathrm{inv}}(\boldsymbol{\chi}^{\mathrm{inv}}) + \Theta^{\mathrm{gm,opr}}(\boldsymbol{\chi}^{\mathrm{inv}}, \boldsymbol{\chi}^{\mathrm{gm,opr}}) + \gamma \tag{1a}$$

subject to:

$$\gamma \geq \Theta^{\mathrm{im,opr}}_{to}(\boldsymbol{\chi}^{\mathrm{inv}}, \boldsymbol{\chi}^{\mathrm{gm,opr}}, \boldsymbol{\chi}^{\mathrm{im,opr}}), \qquad \forall t, o \tag{1b}$$

$$\Phi^{\mathrm{gm,opr}}(\boldsymbol{\chi}^{\mathrm{inv}}, \boldsymbol{\chi}^{\mathrm{gm,opr}}) \leq 0 \tag{1c}$$

$$\Phi^{\mathrm{im,opr}}(\boldsymbol{\chi}^{\mathrm{inv}}, \boldsymbol{\chi}^{\mathrm{gm,opr}}, \boldsymbol{\chi}^{\mathrm{im,opr}}) \leq 0 \tag{1d}$$

where scalar variables are indicated by non-bold symbols while vectors/metrics are indicated by bold symbols. All decision variables related to the investment/reinforcement, grid-connected operation, and islanded operation of the MG are denoted by $\boldsymbol{\chi}^{\mathrm{inv}}$, $\boldsymbol{\chi}^{\mathrm{gm,opr}}$, and $\boldsymbol{\chi}^{\mathrm{im,opr}}$, respectively, i.e., $\boldsymbol{\chi} = [\boldsymbol{\chi}^{\mathrm{inv}}, \boldsymbol{\chi}^{\mathrm{gm,opr}}, \boldsymbol{\chi}^{\mathrm{im,opr}}]$. Also, the auxiliary variable γ is utilized to minimize the operational cost under the worst-case islanding event. Hereafter, the superscripts "gm" and "im" denote the variables that are exclusive to either the grid-connected or the islanded mode, respectively. In the following, the extended formulation of the MG planning problem is presented with only steady-state security constraints.

2.1 Objective Function

2.1.1 Investment: The function $\Theta^{\mathrm{inv}}(\boldsymbol{\chi}^{\mathrm{inv}})$ in (1) is given by:

$$\Theta^{\mathrm{inv}}(\boldsymbol{\chi}^{\mathrm{inv}}) = \sum_{g \in \{\mathcal{S}, \mathcal{C}\}} \left(c^{\mathrm{inv}}_{g} \cdot z_g \right) + \sum_{l \in \mathcal{L}} \left(c^{\mathrm{inv}}_{l} \cdot z_l \right) \tag{2}$$

and includes the total investment/reinforcement costs of generators/lines throughout the planning horizon. Therefore, the investment/reinforcement decision variables include $\boldsymbol{\chi}^{\mathrm{inv}} = \{z_g, z_l\}$.

2.1.2 Grid-connected operation: The function $\Theta^{\mathrm{gm,opr}}$ in (1) capturing the total operational cost in grid-connected mode is defined as:

$$\begin{aligned} \Theta^{\mathrm{gm,opr}}\left(\boldsymbol{\chi}^{\mathrm{gm,opr}}\right) = & \sum_{o \in \mathcal{O}} \sum_{t \in \mathcal{T}} \left(\tau_o \cdot \left(c^{\mathrm{b}}_{to} \cdot p^{\mathrm{gm,b}}_{to} - c^{\mathrm{s}}_{to} \cdot p^{\mathrm{gm,s}}_{to} \right) \right) \\ & + \sum_{o \in \mathcal{O}} \sum_{t \in \mathcal{T}} \sum_{g \in \{\mathcal{S}, \mathcal{C}\}} \left(\tau_o \cdot c_g \cdot p^{\mathrm{gm}}_{gto} \right) \\ & + \sum_{o \in \mathcal{O}} \sum_{t \in \mathcal{T}} \sum_{i \in \mathcal{N}} \left(\tau_o \cdot c^{\mathrm{flx}}_{i} \cdot d^{\mathrm{gm,pf}}_{ito} \right) \end{aligned} \tag{3}$$

where, $\Theta^{\mathrm{gm,opr}}$ includes the total costs of power exchange with the main grid, the total operational costs of generators, and the total penalty costs of shifting power demands away from the periods preferred by consumers.

2.1.3 Islanded operation: The proposed model assumes that MG should be able to withstand an unscheduled islanding event for every hour of each representative day. In the proposed algorithm, MG should adequately supply the power demand for one period (i.e., one hour) after disconnection from the main grid. The function $\Theta^{\mathrm{im,opr}}_{to}$ in (1) capturing the total operational costs in the islanded mode is defined as:

$$\begin{aligned} & \Theta^{\mathrm{im,opr}}_{to}\left(\boldsymbol{\chi}^{\mathrm{im,opr}}\right) = \\ & \qquad \sum_{i \in \mathcal{N}} \left(c^{\mathrm{curt}}_{i} \left(\left(1 - z^{\mathrm{im,pc}}_{ito} \right) d^{\mathrm{im,pc}}_{ito} + \check{d}^{\mathrm{im,pf}}_{ito} \right) \right) \end{aligned} \tag{4}$$

where, $\Theta^{\mathrm{im,opr}}_{to}$ includes the penalty costs for curtailing both constant and flexible power demand while ensuring an adequate power supply to the critical MG loads. The penalty cost c^{curt}_{n} describes the priority level of the load at a specific node where higher values indicate more critical loads.

2.2 Technical Constraints

The constraints that need to be taken into account to reflect operational limitations in the grid-connected and islanded modes are presented below. Where no superscript (i.e., "gm" and "im") is applied to a variable, both the grid-connected and islanded modes are considered.

2.2.1 Constraints on active and reactive power flows: In the proposed MG planning model, the active and reactive power flows

are calculated by (5a)-(5d) based on the conic DistFlow model [27, 28]:

$$P_{l^{i+}to} + p^{\mathrm{gm,b}}_{to|i=1} - p^{\mathrm{gm,s}}_{to|i=1} + \sum_{g\in\{\mathcal{S}^i,\mathcal{C}^i\}} p_{gto} = \sum_{i^-\in\mathcal{N}^i} P_{l^{i-}to} + d^{\mathrm{p}}_{ito}, \quad \forall i,t,o \quad (5a)$$

$$Q_{l^{i+}to} + q^{\mathrm{gm,b}}_{to|i=1} - q^{\mathrm{gm,s}}_{to|i=1} + \sum_{g\in\{\mathcal{S}^i,\mathcal{C}^i\}} q_{gto} = \sum_{i^-\in\mathcal{N}^i} Q_{l^{i-}to} + d^{\mathrm{q}}_{ito}, \quad \forall i,t,o \quad (5b)$$

$$v_{i^-to} = v_{ito} + \left(r^2_{l^{i-}} + x^2_{l^{i-}}\right)\cdot f_{l^{i-}to} + 2\cdot\left(r_{l^{i-}}\cdot P_{l^{i-}to} + x_{l^{i-}}\cdot Q_{l^{i-}to}\right), \quad \forall i,t,o \quad (5c)$$

$$v_{i^-to}\cdot f_{l^{i-}to} \geq \left(P^2_{l^{i-}to} + Q^2_{l^{i-}to}\right), \quad \forall i,t,o \quad (5d)$$

Note that $p^{\mathrm{gm,b/s}}_{to}$ and $q^{\mathrm{gm,b/s}}_{to}$ in (5a) and (5b) are only included for the grid-connected mode at the Point-of-Common Coupling (PCC) node denoted by $i = 1$.

2.2.2 Constraints on power exchange with the main grid: Equations (5e)-(5h) impose the upper limits on the power exchange with the main grid only for the grid-connected mode.

$$0 \leq p^{\mathrm{b,gm}}_{to} \leq \overline{p}^{\mathrm{b}}_{to}\cdot z^{\mathrm{gm,p}}_{to}, \quad \forall t,o \quad (5e)$$

$$0 \leq p^{\mathrm{s,gm}}_{to} \leq \overline{p}^{\mathrm{s}}_{to}\cdot (1 - z^{\mathrm{gm,p}}_{to}), \quad \forall t,o \quad (5f)$$

$$0 \leq q^{\mathrm{b,gm}}_{to} \leq \overline{q}^{\mathrm{b}}_{to}\cdot z^{\mathrm{gm,q}}_{to}, \quad \forall t,o \quad (5g)$$

$$0 \leq q^{\mathrm{s,gm}}_{to} \leq \overline{q}^{\mathrm{s}}_{to}\cdot (1 - z^{\mathrm{gm,q}}_{to}), \quad \forall t,o \quad (5h)$$

where, $z^{\mathrm{gm,p}}_{to}$ and $z^{\mathrm{gm,q}}_{to}$ prevent the simultaneous import and export of active and reactive power, respectively.

2.2.3 Constraints on constant and flexible power demands: Equations (5i)-(5k) reflect the power balance of constant and flexible loads as well as the limitations of flexible loads. For the flexible loads, (5l) limits the allowed energy consumption within each representative day.

$$d^{\mathrm{p}}_{ito} = d^{\mathrm{p_c}}_{ito}\cdot z^{\mathrm{im,p_c}}_{ito} + d^{\mathrm{p_f}}_{ito}, \quad \forall i,t,o \quad (5i)$$

$$d^{\mathrm{q}}_{ito} = d^{\mathrm{q_c}}_{ito}\cdot z^{\mathrm{im,q_c}}_{ito} + d^{\mathrm{q_f}}_{ito}, \quad \forall i,t,o \quad (5j)$$

$$\underline{d}^{\mathrm{p_f}}_{ito} \leq d^{\mathrm{p_f}}_{ito} \leq \overline{d}^{\mathrm{p_f}}_{ito}, \qquad \underline{d}^{\mathrm{q_f}}_{ito} \leq d^{\mathrm{q_f}}_{ito} \leq \overline{d}^{\mathrm{q_f}}_{ito}, \quad \forall i,t,o \quad (5k)$$

$$\sum_{t\in\mathcal{T}} d^{\mathrm{p}}_{ito} = e_{io}, \quad \forall i,o \quad (5l)$$

Note that $z^{\mathrm{im,p_c}}_{ito}$ and $z^{\mathrm{im,q_c}}_{ito}$ in (5i) and (5j) are only included for the islanded mode. The flexible load is further defined during the islanded mode as:

$$d^{\mathrm{im,p_f}}_{ito} = d^{\mathrm{gm,p_f}}_{ito} + \hat{d}^{\mathrm{im,p_f}}_{ito} - \check{d}^{\mathrm{im,p_f}}_{ito}, \quad \forall i,t,o \quad (5m)$$

$$d^{\mathrm{im,q_f}}_{ito} = d^{\mathrm{gm,q_f}}_{ito} + \hat{d}^{\mathrm{im,q_f}}_{ito} - \check{d}^{\mathrm{im,q_f}}_{ito}, \quad \forall i,t,o \quad (5n)$$

$$0 \leq \hat{d}^{\mathrm{im,p_f}}_{ito}, \hat{d}^{\mathrm{im,q_f}}_{ito}, \check{d}^{\mathrm{im,p_f}}_{ito}, \check{d}^{\mathrm{im,q_f}}_{ito}, \quad \forall i,t,o \quad (5o)$$

$$d^{\mathrm{im,p}}_{ito} \leq e_{io} - \sum_{t'=1}^{t-1} d^{\mathrm{p}}_{it'o}, \quad \forall i,t,o \quad (5p)$$

2.2.4 Constraints on power generation of distributed generators: Constraints (5q)-(5t) limit capacities and ramp rates of distributed generators:

$$0 \leq p_{gto} \leq \overline{p}_{gto}\cdot z_g, \quad \forall g,t,o \quad (5q)$$

$$\overline{p}_{gto} = \min(p^{\mathrm{nom}}_g, p^{\mathrm{av}}_{gto}), \quad \forall g,t,o \quad (5r)$$

$$\underline{q}_{gto}\cdot z_g \leq q_{gto} \leq \overline{q}_{gto}\cdot z_g, \quad \forall g,t,o \quad (5s)$$

$$-r^{\mathrm{dn}}_g \leq p_{gto} - p_{g(t-1)o} \leq r^{\mathrm{up}}_g, \quad \forall s,t,o \quad (5t)$$

Note that $\overline{p}_{gto} = p^{\mathrm{nom}}_g$ for SG units while $\overline{p}_{gto} = p^{\mathrm{av}}_{gto}$ for CIG units as the non-fixed maximum available power for each CIG unit is dependent on weather conditions.

2.2.5 Constraints on line thermal limits: The thermal loading of each line is limited by constraint (5u) as given below:

$$P^2_{lto} + Q^2_{lto} \leq \left(\overline{S}_l\right)^2\cdot\left(z^0_l + z_l\right), \quad \forall l,t,o \quad (5u)$$

2.2.6 Constraints on nodal voltage magnitudes: The lower/upper limits on the voltage magnitudes are ensured during the planning horizon as:

$$\underline{v} \leq v_{ito} \leq \overline{v}, \qquad v_{to|i=1} = 1, \quad \forall i,t,o \quad (5v)$$

Here, $\boldsymbol{\chi}^{\mathrm{gm,opr}} = \{d^{\mathrm{gm,p/q}}_{ito}, d^{\mathrm{gm,p_f/q_f}}_{ito}, p^{\mathrm{gm}}_{gto}, P^{\mathrm{gm}}_{lto}, p^{\mathrm{gm,b/s}}_{to}, q^{\mathrm{gm}}_{gto}, Q^{\mathrm{gm}}_{lto}, q^{\mathrm{gm,b/s}}_{to}, v^{\mathrm{gm}}_{ito}\}$ and $\boldsymbol{\chi}^{\mathrm{im,opr}} = \{\hat{d}^{\mathrm{p_f/q_f}}_{ito}, d^{\mathrm{im,p_f/q_f}}_{ito}, \hat{p}_{gto}, p^{\mathrm{im}}_{gto}, P^{\mathrm{im}}_{lto}, \hat{q}_{gto}, q^{\mathrm{im}}_{gto}, Q^{\mathrm{im}}_{lto}, v^{\mathrm{im}}_{ito}\}$.

3 Microgrid Planning with Inertia-Aware Constraints

3.1 Analytic Formulation of the Transient Frequency Security Constraints

The frequency response model adopted in this paper is based on the uniform representation of frequency transients initially introduced in [13] for a traditional system with only SG units. This model is extended in [15], to include SG units (indexed by $i \in \mathcal{S}$) and CIG units (indexed by $c \in \mathcal{C}$). The frequency response model in [15] embeds the most popular frequency control techniques in the literature for *grid-supporting* CIG units providing frequency support i.e., droop (indexed by $d \in \mathcal{C}^d \subseteq \mathcal{C}$) and Virtual Synchronous Machine (VSM) (indexed by $v \in \mathcal{C}^v \subseteq \mathcal{C}$) control strategies [29, 30]. The transfer function $G(s)$ between the active power change $\Delta P_e(s)$ and the CoI frequency deviation $\Delta f(s)$ is derived in [15] as:

$$G(s) = \frac{\Delta f(s)}{\Delta P_e(s)} = \Bigg(\overbrace{(sM_s + D_s)}^{\text{SGs Swing Dynamics}} + \overbrace{\sum_{g\in\mathcal{S}} \frac{K_g(1+sF_gT_g)}{R_g(1+sT_g)}}^{\text{SGs Turbine \& Governor Response}} + \overbrace{\sum_{d\in\mathcal{C}^d} \frac{K_d}{R_d(1+sT_d)}}^{\text{Droop-based CIGs}} + \overbrace{\sum_{v\in\mathcal{C}^v} \frac{sM_v + D_v}{1+sT_v}}^{\text{VSM-based CIGs}} \Bigg)^{-1} \quad (6)$$

where, a positive value of the active power change $\Delta P_e(s)$ corresponds to a net load decrease.

It is worth mentioning that local frequency oscillations result in a distinct transient response at each generator after a disruptive event. However, the dynamic performance characterised by the CoI swing equation using aggregated normalised inertia M and damping D has been shown to provide a smooth overall frequency with investigations illustrating adequate capture of the transient performance of the system [7, 13, 15, 31]. Moreover, the CoI frequency facilitates the provision of better control from CIGs [7, 31].

Since the time constants of all SG units ($T_i \approx T$) are orders of magnitude higher than those of CIG units, it can be assumed that $T \gg T_{d,v} \approx 0$ [32]. Therefore, the transfer function $G(s)$ in (6)

can be approximated as:

$$G(s) = \frac{1}{MT}\frac{1+sT}{s^2+2\zeta\omega_n s+\omega_n^2} \tag{7}$$

where, $\omega_n = \sqrt{\frac{D+R_s}{MT}}$ and $\zeta = \frac{M+T(D+F_s)}{2\sqrt{MT(D+R_s)}}$. Also, other parameters in (7) can be calculated as follows:

$$M_s = \sum_{g\in\mathcal{S}} M_g \frac{P_g}{P_s^{\text{base}}}, \quad D_s = \sum_{g\in\mathcal{S}} D_g \frac{P_g}{P_s^{\text{base}}} \tag{8a}$$

$$R_s = \sum_{g\in\mathcal{S}} \frac{K_g}{R_g}\frac{P_g}{P_s^{\text{base}}}, \quad F_s = \sum_{g\in\mathcal{S}} \frac{K_g F_g}{R_g}\frac{P_g}{P_s^{\text{base}}} \tag{8b}$$

$$M_c = \sum_{v\in\mathcal{C}^v} M_v \frac{P_{c_v}}{P_c^{\text{base}}}, \quad D_c = \sum_{v\in\mathcal{C}^v} D_v \frac{P_{c_v}}{P_c^{\text{base}}} \tag{8c}$$

$$R_c = \sum_{d\in\mathcal{C}^d} R_d \frac{P_{c_d}}{P_c^{\text{base}}} \tag{8d}$$

$$M = \frac{M_s P_s^{\text{base}} + M_c P_c^{\text{base}}}{P_s^{\text{base}} + P_c^{\text{base}}} \tag{8e}$$

$$D = \frac{D_s P_s^{\text{base}} + D_c P_c^{\text{base}} + R_c P_c^{\text{base}}}{P_s^{\text{base}} + P_c^{\text{base}}} \tag{8f}$$

where, P_g and P_c denote the available power reserves of the SG unit g and the CIG unit c, respectively. Furthermore, P_s^{base} and P_c^{base} represent the base power of all SG and CIG units connected to the system, that is, $P_s^{\text{base}} = \sum_{g\in\mathcal{S}} P_g$ and $P_c^{\text{base}} = \sum_{c\in\mathcal{C}} P_c$, respectively.

The dynamic frequency response of the system after a disturbance can be represented by frequency nadir (i.e., $\Delta f^{\max}$) and instantaneous RoCoF (i.e., $\dot{f}^{\max}$). In contrast, the steady-state frequency response of the system can be described by the constant frequency deviation from a pre-disturbance equilibrium (i.e., Δf^{qss}). Given a step-wise disturbance in the active power $\Delta P_e(s) = -\Delta P/s$, where ΔP denotes the net change in the active power, the mathematical expression of the frequency deviation in the time domain (i.e., $\Delta\omega(t) \equiv \Delta f(t)$) can be obtained as follows:

$$\Delta\omega(t) = -\frac{\Delta P}{M}\left(\frac{1}{T\omega_n^2} + \frac{1}{\omega_d}e^{-\zeta\omega_n t}\left(\sin\omega_d t - \frac{1}{\omega_n t}\sin\omega_d t + \phi\right)\right) \tag{9}$$

where, $\omega_d = \omega_n\sqrt{1-\zeta^2}$ and $\phi = \sin^{-1}\left(\sqrt{1-\zeta^2}\right)$.

The frequency nadir occurs at the time instance t_m when $\Delta\dot{\omega}(t_m) \equiv \Delta\dot{f}(t_m) = 0$. Therefore, t_m can be derived by solving $\Delta\dot{\omega}(t_m) \equiv \Delta\dot{f}(t_m) = 0$, and then the frequency nadir can be obtained as given below:

$$\Delta f^{\max} = \Delta f(t_m) = -\frac{\Delta P}{D+R_s}\left(1 + \sqrt{\frac{T(R_s-F_s)}{M}}e^{-\zeta\omega_n t_m}\right) \tag{10}$$

where, $t_m = (1/\omega_d)\tan^{-1}\left(\omega_d/\left(\omega_n\zeta - T^{-1}\right)\right)$.

In addition, the maximum RoCoF occurs at the instance of the disturbance (i.e., $t_r = 0^+$). Therefore, the maximum RoCoF can be obtained by solving $\Delta\dot{\omega}(0^+) \equiv \Delta\dot{f}(0^+)$ as follows:

$$\Delta\dot{f}^{\max} = \Delta\dot{f}(0^+) = -\frac{\Delta P}{M} \tag{11}$$

Finally, the quasi-steady-state frequency deviation can be derived from $\Delta\omega(t) \equiv \Delta f(t)$ in (9) for $t \to \infty$ as given below:

$$\Delta f^{\text{qss}} = \Delta f(\infty) = -\frac{\Delta P}{D+R_s} \tag{12}$$

From (10), (11), and (12), it can be seen that the control parameters M, D, R_s and F_s directly affect the frequency performance of the system. While frequency nadir in (10) is a highly non-linear function of all four system control parameters mentioned above, RoCoF and quasi-steady-state frequency deviation are explicitly affected by M in (11) and both D and R_s in (12), respectively. The above frequency security metrics can be integrated into the MG planning problem to determine cost-effective generation technologies with optimal control parameters to ensure system security in the event of a severe disturbance.

3.2 Formulation of Inertia-Aware Investment Planning Problem

The MG planning model presented in Section 2 can be enhanced to include the transient frequency security constraints, associated with the MG islanding transients. This is accomplished by the inclusion of the frequency metrics defined in (10), (11), and (12) through the addition of the following constraints to the model in (1):

$$\underline{\Delta f}^{\max} \le \Delta f_{to}^{\max} \le \overline{\Delta f}^{\max}, \qquad \forall t, o \tag{13a}$$

$$\underline{\dot{f}}^{\max} \le \dot{f}_{to}^{\max} \le \overline{\dot{f}}^{\max}, \qquad \forall t, o \tag{13b}$$

$$\underline{\Delta f}^{\text{qss}} \le \Delta f_{to}^{\text{qss}} \le \overline{\Delta f}^{\text{qss}}, \qquad \forall t, o \tag{13c}$$

$$\Delta f_{to}^{\max} = -\frac{\Delta P_{to}}{D+R_s}\left(1 + \sqrt{\frac{T(R_s-F_s)}{M}}e^{-\zeta\omega_n t_m}\right), \forall t, o \tag{13d}$$

$$\Delta\dot{f}_{to}^{\max} = -\frac{\Delta P_{to}}{M}, \qquad \forall t, o \tag{13e}$$

$$\Delta f_{to}^{\text{qss}} = -\frac{\Delta P_{to}}{D+R_s}, \qquad \forall t, o \tag{13f}$$

$$\Delta P_{to} = p_{to}^{\text{b/s}}, \qquad \forall t, o \tag{13g}$$

The frequency support provided by a generator g, given its investment status z_g, is a function of its control parameters, i.e., $M(z_g)$, $D(z_g)$, $F_g(z_g)$, and $R_g(z_g)$ in addition to the amount of power exchange with the main grid at the time of islanding, i.e., $\Delta P_{to} = p_{to}^{\text{b/s}}, \forall t \in \mathcal{T}, \forall o \in \mathcal{O}$.

It is essential to note that generators require adequate reserves to provide inertia and primary frequency control. This requirement can be defined by the grid code [33] or calculated by (14) as a function of the maximum acceptable RoCoF $\dot{f}_{\lim}$ and the maximum acceptable frequency deviation $\Delta f_{\lim}$ prior to under-frequency load shedding, respectively:

$$p_g^{\text{res}} = \left(M_g\dot{f}_{\lim} + (D_g + R_g)\Delta f_{\lim}\right) \tag{14}$$

Therefore, the maximum power limit in (5r) for grid-connected operation can be modified to include the reserve requirement as:

$$\overline{p}_{gto}^{\text{gm}} = \min(p_g^{\text{nom}} - p_g^{\text{res}}, p_{gto}^{\text{av}} - p_g^{\text{res}}) \tag{15}$$

While the power and energy reserves for transient frequency control are readily available for SG units based on their capacity, this is not the case for CIG units due to their uncertain power availability. Three technologies can be leveraged for CIG units, i.e., reserves can be provided by: (i) the converter-side DC-link capacitor energy storage [34], (ii) a battery energy storage attached to the CIG [35], or (iii) decreasing the CIG output from the maximum power point to allow for upward regulation. In this paper, the technique detailed in [34] is utilised where the energy and power reserves for transient frequency control of CIG units are provided by the DC-side capacitor.

Now, the inertia-aware MG investment planning problem can be compactly represented as:

$$\min_{\forall\boldsymbol{\chi}} \Theta^{\text{inv}}(\boldsymbol{\chi}^{\text{inv}}) + \Theta^{\text{gm,opr}}(\boldsymbol{\chi}^{\text{inv}}, \boldsymbol{\chi}^{\text{gm,opr}}) + \gamma \tag{16a}$$

subject to:

$$\gamma \geq \Theta_{to}^{\text{im,opr}}(\boldsymbol{\chi}^{\text{inv}}, \boldsymbol{\chi}^{\text{gm,opr}}, \boldsymbol{\chi}^{\text{im,opr}}), \qquad \forall t, o, \tag{16b}$$

$$\Phi^{\text{gm,opr}}(\boldsymbol{\chi}^{\text{inv}}, \boldsymbol{\chi}^{\text{gm,opr}}) \leq 0, \tag{16c}$$

$$\Phi^{\text{im,opr}}(\boldsymbol{\chi}^{\text{inv}}, \boldsymbol{\chi}^{\text{gm,opr}}, \boldsymbol{\chi}^{\text{im,opr}}) \leq 0, \tag{16d}$$

$$\Phi^{\text{fr,opr}}(\boldsymbol{\chi}^{\text{inv}}, \boldsymbol{\chi}^{\text{gm,opr}}, \boldsymbol{\chi}^{\text{fr,opr}}) \leq 0, \tag{16e}$$

where, $\Phi^{\text{fr,opr}}$ incorporates all the constraints in (13) and $\boldsymbol{\chi}^{\text{fr,opr}} = \{M, D, R_s, F_s, \Delta P_{to}\}$.

Although the static operational constraints in the grid-connected and islanded modes are convex, with the inclusion of discrete/continuous investment/operational variables as well as non-linear and non-convex transient security constraints (16e), the investment planning problem described in (16) is a Mixed-Integer Non-Linear Programming (MINLP) problem. To solve this intractable MINLP optimisation problem, two computationally tractable decomposition strategies based on the notion of Benders decomposition are proposed in this paper, as described in more detail in the next section.

4 Proposed Solution Approach for Inertia-aware MG planning

In this section, two decomposition algorithms are proposed, outlining two computationally tractable strategies for solving the inertia-aware MG planning problem in (16) using dual cutting planes. The solution approach in both algorithms is developed based on the notion of Benders decomposition to tackle the MINLP problem in (16) through a four-step iterative procedure, as illustrated in Fig. 1. By applying Benders dual-cutting plane techniques, the problem space of the master problem is iteratively refined through the construction of linear constraints developed from the dual solutions of the sub-problem. In each algorithm, the master problem is related to the MG planning problem under linear static security constraints, while the sub-problem relates to the transient frequency security feasibility. However, the proposed algorithms differ in the formulation of the dual cutting planes as described in Sections 4.1 and 4.2, providing different degrees of freedom that can be leveraged in different applications.

The two-stage problem presented in [25] employs a bound-tightening algorithm that improves the the first-stage investment and operational decisions based on the feasibility of the second-stage problem. However, this technique does not explicitly account for the varying levels of frequency support that different generators can provide based on their control parameters. The algorithms proposed in this paper use the dual solutions of the subproblems which are marginal values that capture the effect of changes in each constraint to the objective. This marginal value quantifies the sensitivity of each generator and/or control parameter to the frequency metrics thereby providing a more meaningful insight from the sub-problem to the master problem. These sensitivities are then applied in the computation of the master problem at the next iteration, therefore, capturing the impact of the optimal decisions of the master problem on the optimal solution of the sub-problem. Both decomposition algorithms are presented in the sequel.

4.1 Bender's Decomposition: An Overview

A general formulation of a Mixed Integer Nonlinear Programming (MINLP) problem can be described as:

$$\phi = \min \quad f(x, y) \tag{17a}$$

$$\text{s.t.} \quad g_j(x, y) \leq 0, \quad \forall j = 1, \ldots, m \tag{17b}$$

$$x \in \mathbb{R}, y \in \mathbb{Z}, \tag{17c}$$

where, x and y denote continuous and integer variables, respectively, while m represent the number of constraints. ϕ is the optimal solution to the problem while the variables take on values (x^*, y^*) at optimality. Decomposition methods exploit the problem structure by

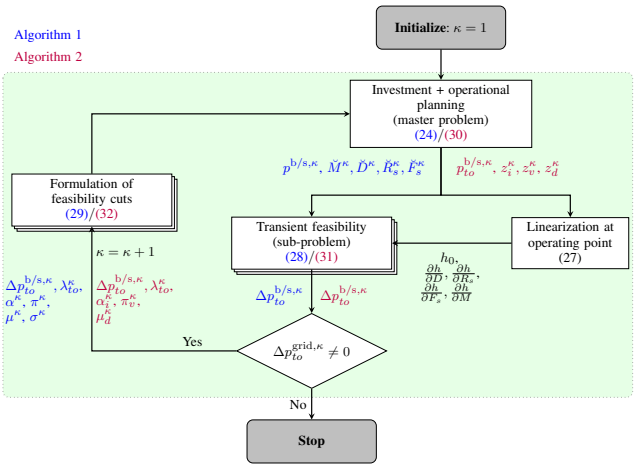

Fig. 1: The proposed decomposition algorithms for the inertia-aware MG planning problem where variables are differentiated with A1 (blue), A2 (purple), and both A1 and A2 (black).

decomposing the large problem into smaller problems that can be solved in parallel or sequentially. The operations common to the different methods for solving MINLPs using such techniques involve two main iterative steps, i.e., first, the relaxation of the problem and second, constraint enforcement and search of the solution space [36]. Constraint enforcement includes search procedures to exclude solutions infeasible to the original (un-relaxed) problem through 'branching' or tightening of the relaxation.

Cutting plane methods are a form of constraint enforcement where the goal is to find if a certain point in the relaxation space Ψ_{rlx} belongs to the feasible set of the un-relaxed problem Ψ. If the solution to the relaxation, denoted here as $(x_{\text{R}}^*, y_{\text{rlx}}^*)$, lies in the feasible space, this is the optimal solution ($x_{\text{rlx}}^* = x^*$, $y_{\text{rlx}}^* = y^*$). Otherwise, a *valid inequality* is generated in the form of a separating hyperplane, which separates the region, where all feasible solutions lie excluding $(x_{\text{rlx}}^*, y_{\text{rlx}}^*)$. If the valid inequality successfully excludes the infeasible solution, it is referred to as a *cut*. The separating hyperplane can then be added as an inequality to the relaxation to tighten the search space.

A problem of the form given in (18), with the variable x, in this case, being a complicating variable* can be complex to solve. Variable y is considered a complicating variable given that when fixed the problem is deomposable.

$$\min_{x,y}\{ax + by : Cx \geq d, f(x, y) \leq 0\} \tag{18}$$

Equation (18) can be reformulated into a tractable form by decomposing it into two simpler problems, i.e., a master and a subproblem.

First, the auxiliary variable α is introduced, thus, defining the master problem of the form:

$$x^* = \min_{x,\alpha}\{ax + \alpha : Cx \geq d, \alpha \geq 0\} \tag{19}$$

The solution to the master problem (19) defines the lower bound of (18). The subproblem is derived as:

$$\min_{\hat{x},y}\{by : f(\hat{x}, y) \leq 0, \hat{x} = x^*\} \tag{20}$$

If the subproblem in (20) is infeasible for the value of x^* obtained from the master problem, a feasibility subproblem must be

*Complicating variables are specific variables in a complex optimization problem preventing a tractable distributed solution if appropriate decomposition strategies are not adopted [37].

formulated. The feasibility subproblem is defined as:

$$\min_{\hat{x},y,\beta}\{\beta : f(\hat{x},y,\beta) \leq 0, \hat{x} = x^*\} \tag{21}$$

From the solution of (21) a feasibility cut defined in (22) is added to the master problem to ensure that infeasible solutions of y^* are excluded from the problem. The dual feasibility cut is defined as:

$$0 \geq \beta^* + (x - \hat{x}^*)\mu, \tag{22}$$

where $\bullet^*$ denotes the optimal value of of the associated variable $\bullet$ and μ is the dual multiplier associated with the constraint $\hat{x} = x^*$.

In the case of feasibility in (20), the solution of the subproblem can then be used by the master problem to obtain an upper-bound solution to the algorithm. A dual optimality cut is added to the problem which is derived as:

$$\alpha \geq By^* + (x - x^*)\mu, \tag{23}$$

The master problems and subproblems are then iteratively solved sequentially until convergence ensues [37].

4.2 Algorithm 1

In Algorithm 1 (A1), the complicating variables between the master problem and the sub-problem are the power exchange of the MG with the main grid (i.e., $p_{to}^{\mathrm{b/s}}$) and frequency control parameters for different generators (i.e., $\breve{M}_s$, $\breve{D}_s$, $\breve{F}_s$, and $\breve{R}_s$ for SGs, $\breve{M}_c$, $\breve{D}_c$, and $\breve{R}_c$ for CIGs, and $\breve{M}$ and $\breve{D}$ for both SGs and CIGs). The accent $\breve{}$ is used to differentiate a non-normalised parameter $\bullet$ from its normalised counterpart $\breve{\bullet}$. The tasks at each iteration in A1 are detailed as follows:

Step 1) Initial Formulation of the Master Problem: Initially, at iteration $\kappa = 1$, the master problem, which is a relaxation of (1), is solved to obtain feasible values of the complicating variables. It can be formulated as given below:

$$\min_{\boldsymbol{\chi}} \ \Theta^{\mathrm{inv}}(\boldsymbol{\chi}^{\mathrm{inv}}) + \Theta^{\mathrm{gm,opr}}(\boldsymbol{\chi}^{\mathrm{inv}}, \boldsymbol{\chi}^{\mathrm{gm,opr}}) + \gamma \tag{24a}$$

subject to:

$$\gamma \geq \Theta_{to}^{\mathrm{im,opr}}(\boldsymbol{\chi}^{\mathrm{inv}}, \boldsymbol{\chi}^{\mathrm{gm,opr}}, \boldsymbol{\chi}^{\mathrm{im,opr}}), \quad \forall t, o \tag{24b}$$

$$\Phi^{\mathrm{gm,opr}}(\boldsymbol{\chi}^{\mathrm{inv}}, \boldsymbol{\chi}^{\mathrm{gm,opr}}) \leq 0 \tag{24c}$$

$$\Phi^{\mathrm{im,opr}}(\boldsymbol{\chi}^{\mathrm{inv}}, \boldsymbol{\chi}^{\mathrm{gm,opr}}, \boldsymbol{\chi}^{\mathrm{im,opr}}) \leq 0 \tag{24d}$$

$$\breve{M}_s = \sum_{g\in\mathcal{S}} M_g P_g z_g, \qquad \breve{D}_s = \sum_{g\in\mathcal{S}} D_g P_g z_g \tag{24e}$$

$$\breve{R}_s = \sum_{g\in\mathcal{S}} \frac{K_g}{R_g} P_g z_g, \qquad \breve{F}_s = \sum_{g\in\mathcal{S}} \frac{K_g F_g}{R_g} P_g z_g \tag{24f}$$

$$\breve{M}_c = \sum_{v\in\mathcal{C}^v} M_v P_{c_v} z_v \quad \breve{D}_c = \sum_{v\in\mathcal{C}^v} D_v P_{c_v} z_v \tag{24g}$$

$$\breve{R}_c = \sum_{d\in\mathcal{C}^d} R_d P_{c_d} z_d \tag{24h}$$

$$\breve{M} = \breve{M}_s + \breve{M}_c, \qquad \breve{D} = \breve{D}_s + \breve{D}_c + \breve{R}_c \tag{24i}$$

$$P^{\mathrm{base}} = P_s^{\mathrm{base}} + P_c^{\mathrm{base}} = \sum_{g\in\mathcal{S}} P_g z_g + \sum_{c\in\mathcal{C}} P_c z_c \tag{24j}$$

where, the vector $\boldsymbol{\chi}$ includes all investment variables (i.e., $z_g, \forall g \in \mathcal{S}$, $z_v, \forall v \in \mathcal{C}^v$, $z_d, \forall d \in \mathcal{C}^d$, and $z_c = \{z_v, z_d\}$). The proposed master problem (24) for A1 as a Mixed-Integer Linear Programming (MILP) problem can be solved by available optimisation packages straightforwardly.

Step 2) Linearisation at Each Operating Point: The nadir constraint (13a) is highly non-linear and non-convex. To remedy this issue, before its application to the sub-problem, it is linearised around the operating point at each hour of every representative day (i.e., $\forall t \in \mathcal{T}$ and $\forall o \in \mathcal{O}$). For this purpose, $\Delta f_{to}^{\max}$ in (13d) can be rewritten as follows:

$$\Delta f_{to}^{\max} = \frac{p_{to}^{\mathrm{b/s}}}{h\left(D, R_s, F_s, M\right)} \tag{25}$$

where:

$$h\left(D, R_s, F_s, M\right) = \frac{1}{\frac{1}{D+R_s}\left(1 + \sqrt{\frac{T(R_s - F_s)}{M}} e^{-\zeta\omega_n t_m}\right)} \tag{26}$$

Now, Taylor expansion is utilised to linearise the nadir constraint (13a) at each iteration as given below:

$$\tilde{h}\underline{\Delta f}^{\max} \leq p_{to}^{\mathrm{b/s}} \leq \tilde{h}\overline{\Delta f}^{\max} \tag{27a}$$

$$\begin{aligned} h \approx \tilde{h} = h_0^{\kappa} &+ \frac{\partial h}{\partial D}(D - D^{\kappa}) + \frac{\partial h}{\partial R_s}(R_s - R_s^{\kappa}) \\ &+ \frac{\partial h}{\partial F_s}(F_s - F_s^{\kappa}) + \frac{\partial h}{\partial M}(M - M^{\kappa}) \end{aligned} \tag{27b}$$

where, $\tilde{h}$ is an auxiliary variable, and hereafter, the superscript κ is used to differ fixed variables (e.g., D^{κ}) from non-fixed variables (e.g., D) at iteration κ of the decomposition algorithm. The Taylor expansion introduces an approximation error that lowers the accuracy of the expression. The proximity between the true and approximate expressions (i.e., $\Delta f_{\mathrm{exact}}^{\max,\kappa}$ and $\Delta f_{\mathrm{approx}}^{\max,\kappa}$, respectively) is computed using the absolute error $\epsilon_{\mathrm{abs}} = |\Delta f_{\mathrm{exact}}^{\max,\kappa} - \Delta f_{\mathrm{approx}}^{\max,\kappa}|$ and the relative error $\epsilon_{\mathrm{rel}} = \frac{|\Delta f_{\mathrm{exact}}^{\max,\kappa} - \Delta f_{\mathrm{approx}}^{\max,\kappa}|}{\Delta f_{\mathrm{exact}}^{\max,\kappa}}$. Application of these metrics to the above first-order approximation for 1000 scenarios indicated $\epsilon_{\mathrm{abs}} = 4.7878 \times 10^{-4}$ and $\epsilon_{\mathrm{rel}} = 0.2734\%$ on average. Although higher-order approximations can be employed for higher accuracy, they can result in the non-linearity and non-convexity of the optimisation problem and further complexity. Also, the dynamic simulations indicated in the preceding sections further provide guarantees on the efficacy of the first-order approximation.

Step 3) Formulation of the Sub-Problem: To check whether the transient security constraints in (13) are satisfied based on the solution of the master problem at each iteration or not, feasibility sub-problems are formulated. Given optimal values of complicating variables obtained from solving the master problem at iteration k (e.g., $p_{to}^{\mathrm{b/s},\kappa}$), the sub-problem for each hour t of every representative day o can be formulated as a Linear Programming (LP) problem using the slack variable $\Delta p_{to}^{\mathrm{b/s}}$ as given below:

$$\min_{\Delta p_{to}^{\mathrm{b/s}}} \ |\Delta p_{to}^{\mathrm{b/s}}| \tag{28a}$$

subject to:

$$\tilde{h}\underline{\Delta f}^{\max} \leq p_{to}^{\mathrm{b/s}} + \Delta p_{to}^{\mathrm{b/s}} \leq \tilde{h}\overline{\Delta f}^{\max} \tag{28b}$$

$$\begin{aligned} \tilde{h} = h_0^{\kappa} &+ \frac{\partial h}{\partial D}\frac{(D - \breve{D}^{\kappa})}{P^{\mathrm{base},\kappa}} + \frac{\partial h}{\partial R_s}\frac{(R_s - \breve{R}_s^{\kappa})}{P_s^{\mathrm{base},\kappa}} \\ &+ \frac{\partial h}{\partial F_s}\frac{(F_s - \breve{F}_s^{\kappa})}{P_s^{\mathrm{base},\kappa}} + \frac{\partial h}{\partial M}\frac{(M - \breve{M}^{\kappa})}{P^{\mathrm{base},\kappa}} \end{aligned} \tag{28c}$$

$$\tilde{i}\underline{f}^{\max} \leq p_{to}^{\mathrm{b/s}} + \Delta p_{to}^{\mathrm{b/s}} \leq \tilde{i}\overline{f}^{\max} \tag{28d}$$

$$\tilde{i} = \frac{M}{P^{\mathrm{base},\kappa}} \tag{28e}$$

$$\tilde{j}\underline{\Delta f}^{\mathrm{qss}} \leq p_{to}^{\mathrm{b/s}} + \Delta p_{to}^{\mathrm{b/s}} \leq \tilde{j}\overline{\Delta f}^{\mathrm{qss}} \tag{28f}$$

$$\tilde{j} = \frac{D}{P^{\text{base},\kappa}} + \frac{R_s}{P_s^{\text{base},\kappa}} \tag{28g}$$

$$p_{to}^{\text{b/s}} = p_{to}^{\text{b/s},\kappa} \quad (\text{dual } \lambda_{to}) \tag{28h}$$

$$M = \breve{M}^{\kappa} \quad (\text{dual } \alpha) \tag{28i}$$

$$D = \breve{D}^{\kappa} \quad (\text{dual } \pi) \tag{28j}$$

$$R_s = \breve{R}_s^{\kappa} \quad (\text{dual } \mu) \tag{28k}$$

$$F_s = \breve{F}_s^{\kappa} \quad (\text{dual } \sigma) \tag{28l}$$

where, the auxiliary variables $\tilde{h}$ in (28b)-(28c), $\tilde{i}$ in (28d)-(28e), and $\tilde{j}$ in (28f)-(28g) are used to include the constraints (13a) and (13d), constraints (13b) and (13e), and constraints (13c) and (13f), respectively, in the sub-problem without any non-linear term. Also, λ_{to}, α, π, μ and σ are dual variables for the constraints fixing the complicating variables (i.e., the power exchange with the main grid, aggregated inertia, damping, droop, and turbine power fraction, respectively) in the sub-problem. These dual variables provide the sensitivity of the optimal solution obtained from solving the sub-problem to the optimal values of the complicating variables obtained from solving the master problem.

If the optimal solution in (28) is equal to zero for all hours of all representative days, this implies the feasibility of the master problem. In this case, A1 is terminated, and the solution of the master problem at the final iteration is the optimal solution. On the other hand, if the optimal solution in (28) is non-zero for even one hour of a specific representative day, i.e., $\exists|\Delta p_{to}^{\text{b/s}}| > 0$, this implies the infeasibility of the sub-problem given the values of the complicating variables. Physically, this is associated with violations of transient security constraints. To eliminate these violations, feasibility cuts are added to the master problem.

Step 4) Formulation of Resilient Feasibility Cut: Given the dual variables obtained from solving each sub-problem at iteration κ (i.e., λ_{to}^{κ}, α^{κ}, π^{κ}, μ^{κ}, and σ^{κ}), the master problem in (24) is updated with the dual cutting planes if the sub-problem in (28) is infeasible, i.e., $\exists|\Delta p_{to}^{\text{b/s},\kappa}| > 0$. The cutting planes added to the master problem are defined as follows:

$$\begin{aligned}\Delta p_{to}^{\text{grid},\kappa} &+ \lambda_{to}^{\kappa}(p_{to}^{\text{b/s}} - p_{to}^{\text{b/s},\kappa}) + \alpha^{\kappa}(\breve{M} - \breve{M}^{\kappa}) \\ &+ \pi^{\kappa}(\breve{D} - \breve{D}^{\kappa}) + \mu^{\kappa}(\breve{R}_s - \breve{R}_s^{\kappa}) \\ &+ \sigma^{\kappa}(\breve{F}_s - \breve{F}_s^{\kappa}) \leq 0, \qquad \forall t, o, \kappa\end{aligned} \tag{29}$$

The dual cutting planes in A1 are associated with the grid power exchange and the unit control parameters. This implies that the sufficiency of frequency support is examined based on the level of the power exchange with the main grid ($p_{to}^{\text{b/s}}$) in addition to the aggregated levels of inertia (M) and damping (D) of CIG and SG units plus the droop support (R_s) and the turbine power fraction (F_s) of SG units.

4.3 Algorithm 2

Differing from A1, the complicating variables in Algorithm 2 (A2) are defined by the investment status of different units (i.e., $z_g, \forall g \in \mathcal{S}$, $z_v, \forall v \in \mathcal{C}^v$, $z_d, \forall d \in \mathcal{C}^d$, and $z_c = \{z_v, z_d\}$) and the power exchange with the main grid (i.e., $p_{to}^{\text{b/s},\kappa}, \forall t \in \mathcal{T}, \forall o \in \mathcal{O}$).

The tasks at each iteration in A2 are detailed as follows:

Step 1) Initial Formulation of the Master Problem: At iteration $\kappa = 1$, the feasible values of the complicating variables are obtained from the MILP master problem as a relaxation of (1) formulated as follows:

$$\min_{\boldsymbol{\chi}} \ \Theta^{\text{inv}}(\boldsymbol{\chi}^{\text{inv}}) + \Theta^{\text{gm,opr}}(\boldsymbol{\chi}^{\text{inv}}, \boldsymbol{\chi}^{\text{gm,opr}}) + \gamma \tag{30a}$$

subject to:

$$\gamma \geq \Theta_{to}^{\text{im,opr}}(\boldsymbol{\chi}^{\text{inv}}, \boldsymbol{\chi}^{\text{gm,opr}}, \boldsymbol{\chi}^{\text{im,opr}}), \ \forall t, o \tag{30b}$$

$$\Phi^{\text{gm,opr}}(\boldsymbol{\chi}^{\text{inv}}, \boldsymbol{\chi}^{\text{gm,opr}}) \leq 0 \tag{30c}$$

$$\Phi^{\text{im,opr}}(\boldsymbol{\chi}^{\text{inv}}, \boldsymbol{\chi}^{\text{gm,opr}}, \boldsymbol{\chi}^{\text{im,opr}}) \leq 0 \tag{30d}$$

$$P^{\text{base}} = P_s^{\text{base}} + P_c^{\text{base}} = \sum_{g\in\mathcal{S}} P_g z_g + \sum_{c\in\mathcal{C}} P_c z_c \tag{30e}$$

Step 2) Linearisation: The linearisation step is undertaken similarly to A1 and the result is applied to the sub-problem.

Step 3) Formulation of the Sub-Problem: The feasibility of the master problem defined in (30) is evaluated using the sub-problems described as follows:

$$\min_{\Delta p_{to}^{\text{b/s},\kappa}} \ |\Delta p_{to}^{\text{b/s},\kappa}| \tag{31a}$$

subject to:

$$\tilde{h}\underline{\Delta f}^{\max} \leq p_{to}^{\text{b/s}} + \Delta p_{to}^{\text{b/s}} \leq \tilde{h}\overline{\Delta f}^{\max} \tag{31b}$$

$$\begin{aligned}\tilde{h} = h_0^{\kappa} &+ \frac{\partial h}{\partial D}(D - \breve{D}^{\kappa}) + \frac{\partial h}{\partial R_s}(R_s - \breve{R}_s^{\kappa}) \\ &+ \frac{\partial h}{\partial F_s}(F_s - \breve{F}_s^{\kappa}) + \frac{\partial h}{\partial M}(M - \breve{M}^{\kappa})\end{aligned} \tag{31c}$$

$$\tilde{i}\underline{f}^{\max} \leq p_{to}^{\text{b/s}} + \Delta p_{to}^{\text{b/s}} \leq \tilde{i}\overline{f}^{\max} \tag{31d}$$

$$\tilde{i} = M, \tag{31e}$$

$$\tilde{j}\underline{\Delta f}^{\text{qss}} \leq p_{to}^{\text{b/s}} + \Delta p_{to}^{\text{b/s}} \leq \tilde{j}\overline{\Delta f}^{\text{qss}} \tag{31f}$$

$$\tilde{j} = D + R_s \tag{31g}$$

$$M_s = \sum_{g\in\mathcal{S}} M_g \frac{P_g}{P_s^{\text{base},\kappa}} z_g, \quad D_s = \sum_{g\in\mathcal{S}} D_g \frac{P_g}{P_s^{\text{base},\kappa}} z_g \tag{31h}$$

$$R_s = \sum_{i\in\mathcal{S}} \frac{K_g}{R_g} \frac{P_g}{P_s^{\text{base},\kappa}} z_g, \quad F_s = \sum_{i\in\mathcal{S}} \frac{K_g F_g}{R_g} \frac{P_g}{P_s^{\text{base},\kappa}} z_g \tag{31i}$$

$$M_c = \sum_{v\in\mathcal{C}^v} M_v \frac{P_{c_v}}{P_c^{\text{base},\kappa}} z_v, \ D_c = \sum_{v\in\mathcal{C}^v} D_v \frac{P_{c_v}}{P_c^{\text{base},\kappa}} z_v \tag{31j}$$

$$R_c = \sum_{d\in\mathcal{C}^d} R_d \frac{P_{c_d}}{P_c^{\text{base},\kappa}} z_d \tag{31k}$$

$$M = \frac{M_s P_s^{\text{base},\kappa} + M_c P_c^{\text{base},\kappa}}{P_s^{\text{base},\kappa} + P_c^{\text{base},\kappa}} \tag{31l}$$

$$D = \frac{D_s P_s^{\text{base},\kappa} + D_c P_c^{\text{base},\kappa} + R_c P_c^{\text{base},\kappa}}{P_s^{\text{base},\kappa} + P_c^{\text{base},\kappa}} \tag{31m}$$

$$p_{to}^{\text{b/s}} = p_{to}^{\text{b/s},\kappa} \quad (\text{dual } \lambda_{to}) \tag{31n}$$

$$z_g = z_g^{\kappa} \quad \forall g \quad (\text{dual } \alpha_g) \tag{31o}$$

$$z_v = z_v^{\kappa} \quad \forall v \quad (\text{dual } \pi_v) \tag{31p}$$

$$z_d = z_d^{\kappa} \quad \forall d \quad (\text{dual } \mu_d) \tag{31q}$$

where, λ_{to}, α_g, π_v, and μ_d are dual variables for the constraints fixing the complicating variables (i.e., the power exchange with the main grid, and investment status of SG and CIG units with VSM and droop control, respectively) in the sub-problem.

Step 4) Formulation of Resilient Feasibility Cut: Given the dual variables obtained from solving each sub-problem at iteration κ (i.e., λ_{to}^{κ}, α_i^{κ}, π_v^{κ}, and μ_d^{κ}), the master problem in (30) is updated with the dual cutting planes if the sub-problem in (31) is infeasible, i.e., $\exists|\Delta p_{to}^{\text{b/s},\kappa}| > 0$. The cutting planes added to the master problem are

defined as follows:

$$\Delta p_{to}^{\mathrm{b/s},\kappa} + \lambda_{to}^{\kappa}(p_{to}^{\mathrm{b/s}} - p_{to}^{\mathrm{b/s},\kappa}) + \sum_{g\in\mathcal{S}} \alpha_g^{\kappa}(z_g - z_g^{\kappa}) + \sum_{v\in\mathcal{C}^v} \pi_v^{\kappa}(z_v - z_v^{\kappa}) + \sum_{d\in\mathcal{C}^d} \mu_d^{\kappa}(z_d - z_d^{\kappa}) \leq 0,\ \forall t, \forall o. \tag{32}$$

The dual cutting planes in A2 are associated with the grid power exchange and the investment status of different units. Therefore, the feasibility and sufficiency of the frequency support depend on the level of the power exchange with the main grid ($p_{to}^{\mathrm{b/s}}$) and the level of support offered by different invested units (z_g, z_v, and z_d).

Both models can obtain an optimal solution as discussed in Section 5. In both A1 and A2, the master problem is MILP while the sub-problem is LP. These are tractable reformulations of the MINLP problem in (1) and can be easily solved with available off-the-shelf optimisation solvers. Fig. 1 summarises the proposed algorithms.

5 Case Study Results

In this section, the proposed algorithms are tested and verified on an 18-bus [25] LV network and a 30-bus [38, 39] MV network under various operating scenarios. Detailed configurations and network parameters for the LV and MV networks can be found in [25] and [38] respectively. Both networks include one already existing SG indicated as SG_1 units as well as four types of candidate investment units, i.e., one SG unit (SG_2), two *grid-supporting* Photovoltaic (PV) CIG units (PV_1, PV_2), and one PV CIG unit (PV_3) operating in *grid-feeding* mode with fixed power output. Candidates PV_1 and PV_2 provide VSM and droop control, respectively. The generator parameters are as described in Table 1.

The 18-bus LV network has one pre-installed SG unit at node one and four investment candidates at nodes $\{15, 17, 11, 18\}$ (see Fig. 2 in [25]) that include one SG unit (SG_2), one VSM-based CIG unit (PV_1), one droop-based CIG unit (PV_2), and one fixed power output CIG unit (PV_3). The 30-bus MV network consists of one pre-installed SG unit at node one and seven investment candidate units at nodes $=\{3, 6, 12, 18, 24, 27\}$ (see Fig. 3 in [39]). The candidate units include one SG unit (SG_2), two VSM-based CIG units (PV_1), two droop-based CIG units (PV_2), and two fixed power output CIG units (PV_3). The annualised investment and operation costs applied in the planning problem are defined in [25] and derived from [40, 41]. The calculations for annualised costs account for the interest rate and lifetime of the generation unit, i.e., 30 years for the solar PV.

The transient frequency security constraints are enforced through thresholds imposed on frequency nadir ($\overline{\Delta f}^{\max} = -\underline{\Delta f}^{\max} = 0.6\,\mathrm{Hz}$), RoCoF ($\overline{\dot{f}}^{\max} = -\underline{\dot{f}}^{\max} = 2\,\mathrm{Hz/s}$), and quasi-steady-state frequency deviation ($\overline{\Delta f}^{\mathrm{qss}} = -\underline{\Delta f}^{\mathrm{qss}} = 0.2\,\mathrm{Hz}$). Further network parameters can be found in [25]. The implementation is undertaken using MATLAB, where the optimisation model formulated in YALMIP [42] and solved by GUROBI [43].

Four case studies are presented to verify the performance of the proposed models as follows:

–**Base**: The benchmark MG planning model considering only static constraints in pre- and post-islanded modes (similar to techniques in [40, 44–47]);
–**Algorithm 0 (A0)**: The MG planning model considering both static and transient frequency security constraints using sequential linearisation and bounds tightening [25];
–**A1**: The proposed MG planning model considering both static and transient frequency security constraints using the decomposition-based algorithm in Section 4.2;
–**A2**: The proposed MG planning model considering both static and transient frequency security constraints using the decomposition-based algorithm in Section 4.3.

Table 1 Investment Costs and Frequency Support Parameters for the Considered Generator Units.

	SG_1	SG_2	PV_1	PV_2	PV_3
Annualised investment cost (\$/kW)	-	140	200	185	170
M (s)	14	14	14	-	-
D (p.u.)	0.9	0.9	0.9	-	-
K (p.u.)	1	1	1	1	-
R (p.u.)	0.03	0.03	-	0.05	-
F (p.u.)	0.35	0.35	-	-	-
Existing generator					
Candidate generators					

5.1 Planning Costs

The models are initially tested on the 18-bus LV network where the costs and planning decisions considering four representative days are compared with each of the three algorithms A0, A1, and A2, as indicated in Table 2. The representative days where extracted from the historical data of yearly patterns of loads and PV generation in Texas for the year 2016 [48]. With all algorithms, there exists an increment in total costs compared to the Base case. For A0, a 10% increment in total costs is observed, compared to an 8.8% increment for A1 and A2. The total investment costs are lowest with A0 compared to A1 and A2 while the solution for A0 results in the highest operational costs. When transient frequency security constraints are applied to the problem (A0, A1, and A2), it is essential that the algorithm minimises costs while ensuring that the level of frequency support in the network is adequate to eliminate violations. Recall that the transient frequency response depends on the aggregated levels of parameters M, D, R_s, and F_s provided by the installed units (see (8e) and (8f)). While the installed capacity is similar for algorithms A0, A1, and A2, as depicted in Table 2, the support offered by the selected CIG units varies.

Compared to the Base case, A0 selects an additional droop-based CIG unit (PV_2) only contributing to the aggregated damping level while A1 and A2 select an additional VSM-based CIG unit (PV_1) contributing to both the aggregated damping and inertia levels (see (8e) and (8f)). Droop-based CIG units contribute to frequency support only in the region of primary frequency response and not during inertia response. As more frequency support is available from the units selected by A1 and A2, the preventive operational actions are kept to a minimum. The solution provided by A0 considers the cheapest investment unit while A1 and A2 select the most *cost-effective* unit. Unlike A0, the decomposition approach used in A1 and A2 provides sensitivity information from the sub-problem to the master problem resulting in a solution that is not only optimal in cost but also ensures optimal frequency support.

5.2 Dynamic Performance

Based on the units installed by each algorithm, the total aggregated level of M and D are 7.84 s and 18 p.u. for A0 as compared to 17.64 s and 1.13 p.u. for A1 and A2. Fig. 2 presents a box plot that

Table 2 Comparison of optimal costs and decisions, inertia support, and computational performance for each algorithm using four representative days.

	Base	**Algorithm 0**	**Algorithm 1**	**Algorithm 2**
Costs and decisions				
Total cost (\$)	223390	244780	242740	242740
Investment cost (\$)	61000	126000	131000	131000
Investment decisions	PV_3	PV_2, PV_3	PV_1, PV_3	PV_1, PV_3
Operational cost (\$)	162390	118780	111740	111740
Demand shift penalty (\$)	3675	8468	7787	7787
Frequency support				
M (s)	7.84	7.84	17.64	17.64
D (p.u)	0.50	18.00	1.13	1.13

indicates the variations in the measured values for each of the frequency security metrics for the 96 hours in four representative days. The security limit in each case is indicated by the dotted red line.

In the case of the nadir values, averages of 49.77 Hz and 49.70 Hz are recorded in A0 and A1/A2, respectively (see Fig. 2a), as compared to the Base case where an average of 49.55 is obtained. The variation of nadir in A0 indicates a smaller range as compared to A1/A2 with a slightly improved performance. In the case of the RoCoF values, depicted in Fig. 2b, an average of 1.59 Hz/s is achieved for A0 as compared to 0.79 Hz/s for A1 and A2. RoCoF is mainly dependent on the total inertia level (M) present in the network (see (11)). The solution provided by A0 provides an inertia level of 7.84 s, provided mainly by the pre-installed SG. The results based on A1 and A2 include the additional installation of VSM-based unit PV_1 resulting in an inertia level of 17.64 s, and therefore, a better performance level compared to A0. On the other hand, the quasi-steady-state frequency is dependent on the aggregated D and R_s parameters, as indicated in (12). In Fig. 2c, the averages of 49.89 Hz and 49.87 Hz are observed for A0 and A1/A2,

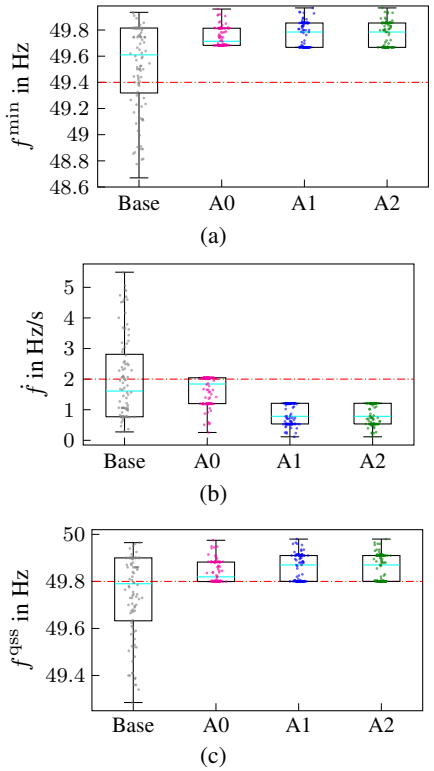

Fig. 2: Distribution of (a) nadir, (b) RoCoF, and (c) quasi-steady-state frequency for each algorithm considering all hours in four representative days.

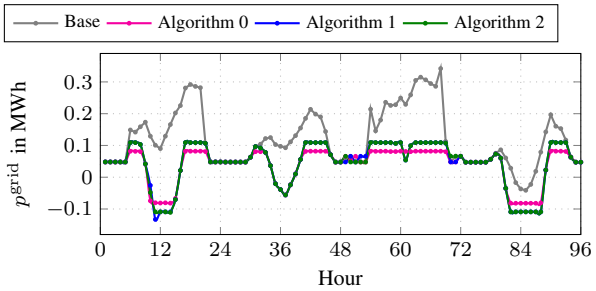

Fig. 3: Impact of the transient frequency constraints on active power exchange with the main grid for the different algorithms (-/+ indicate power export/import).

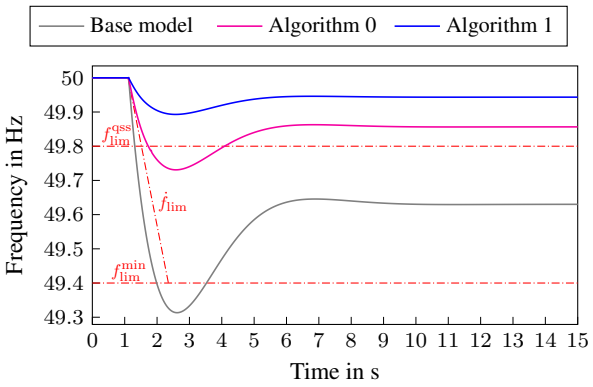

Fig. 4: Evolution of the CoI frequency for 15 seconds after disconnection of the MG from the main grid at hour 68.

respectively. From Table 2, it can be seen that the aggregated damping levels are higher with the units installed by the A0 solution hence providing slightly better performance.

The impact of the inclusion of transient constraints on the active power exchange with the main grid is shown in Fig. 3. All the algorithms provide a solution that is robust to the loss of power exchange with the main grid in every operation scenario. For the MG, the power exchange with the main grid is usually the largest power injection, the loss of this power exchange may result in large frequency excursions. A0 explicitly restricts the bounds on the grid power exchange at each hour while A1 and A2 vary the dispatch based on the sensitivities to both the power loss and available inertia. The result of A0 is shown to be more conservative compared to A1 and A2. This is especially due to the lack of bidirectional information exchange between the problems at each stage. A0 only restricts power exchange based on the feasibility of the transient frequency security problem, without knowledge of the impact of different control parameters on the transient frequency security. It is noteworthy to mention that during instances of power import, the disconnection from the main grid can result in potential under-frequency, while for power export, over-frequencies can be recorded.

The analytical performance, shown in Fig. 2, is further validated using time-domain simulations. Given the optimal solution provided by the Base case, A0, and A1 (A2 is omitted since it has the same solution as A1), Fig. 4 indicates the frequency trajectories for the operational scenario at hour 68 out of 96 operational hours in four representative days. Note that based on Fig. 3, this hour represents the highest power exchange from the grid, and thus, the worst-case mismatch in power if the MG is disconnected. The superiority of A1 over A0 is further validated in Fig. 4 which compares the frequency trajectories of each technique using a time domain simulation. The dynamic simulation is performed with PyRAMSES [49] with the grid disconnection occurring at time $t = 1$ s and the dotted red lines have been used to indicate the transient frequency security limits. While in this scenario, all metrics of A1 show a better performance than A0, this may however not always be the case as indicated in Fig. 2. The frequency evolution is dependent on both the level of power mismatch at the instant of disconnection dictated by the hourly power exchange and the control support available.

5.3 Sensitivity to Variation in Security Limits

Tightening the limits, i.e., reducing the upper bounds and increasing the lower bounds, increases the system requirement on power reserves necessary for frequency support from the system. In this paper, three case studies are defined to analyse the effect of threshold variations, i.e.:

1. Case A: denotes the initially considered limits
2. Case B: denotes the tightening of *only* the RoCoF limit
3. Case C: denotes the tightening of *only* the quasi-steady-state frequency limit

Table 3 Planning decisions obtained from the algorithms with tighter transient security bounds on RoCoF (Case B: Tightening RoCoF to 0.5 Hz/s).

	Algorithm 0	Algorithm 1	Algorithm 2
Costs and decisions			
Total cost ($)	302790	295303	295319
Investment decisions	PV_2, PV_3, SG_2	PV_1, PV_3, SG_2	PV_1, PV_3, SG_2

Table 4 Planning decisions obtained from the algorithms with tighter transient security bounds on quasi-steady-state frequency (Case C: Tightening quasi-steady-state frequency deviation limit to 0.1 Hz).

	Algorithm 0	Algorithm 1	Algorithm 2
Costs and decisions			
Total cost ($)	296734	296665	296665
Investment decisions	PV_2, PV_3, SG_2	PV_2, PV_3, SG_2	PV_2, PV_3, SG_2

Higher support requirements can be met by further leveraging high-cost preventive actions. If, however, the current system configuration fails to meet the security requirements, new units can be installed to increase support levels. Furthermore, as shown in (10)-(12), the different metrics are dependent on either one or a combination of different control parameters. Hence, the commitment of a generator will depend on its suitability to enhance performance. The effect of the security limit restriction on the aggregated damping and inertia magnitudes is presented in Fig. 5, while the sensitivity of the planning solutions to threshold variations is presented in Tables 3 and 4 and Fig. 6.

In Case B, the RoCoF thresholds are reduced from 2 Hz/s to 0.5 Hz/s. From (11), RoCoF is more dependent on the aggregated inertia M. Fig. 5 indicates an increase in inertia levels for all algorithms. A significant increment to 34.66 s with A1/A2 as compared to 17.64 s in Case A is shown while a lower increment of 22.28 s is obtained with A0. While all algorithms present the need to install an additional unit as indicated in Table 3, units installed with A0 include a droop-based generator that has no contribution to the aggregated inertia M. Hence, A0 resorts to more expensive preventative actions to further eliminate transient security violations increasing total costs as detailed in Fig. 6.

In Case C, the quasi-steady-state frequency deviation bound is reduced from 0.2 Hz to 0.1 Hz. From (12), the quasi-steady-state frequency is dependent on the magnitude of control parameters for damping and droop. In Fig. 5, damping levels for Case C with A1/A2 are shown to increase from 1.13 p.u. in Case A to 23.54 p.u. in Case C. Note that in Case C, the units installed with A1/A2 include a droop-based CIG PV_2 instead of VSM-based PV_1 (see Table 4) as in Case A and B. This is due to the higher requirement for damping support with Case C as compared to Case A necessitating the adoption of units that result in better performance.

The results presented in Tables 3 and 4 as well as Fig. 5 further indicate the need for sensitivity information exchange between the two stages of the algorithm, i.e., the master problem and the sub-problem. This simultaneously optimises both frequency support and system costs as highlighted by the superiority of the solution obtained with A1 and A2 as compared to A0.

The application of tighter security limits is associated with a sharp increase in costs as further detailed in Fig. 6. For A0, while cheaper investments are taken for Case B, there is a higher reliance on expensive operational measures such as demand-shifting to ensure security restrictions are met. On the other hand, algorithms A1 and A2 require more expensive inertia-supporting units resulting in higher investment costs but fewer operational measures are taken hence resulting in a lower overall cost as compared to A0.

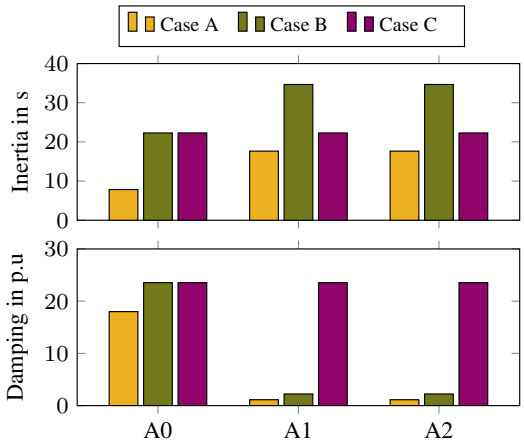

Fig. 5: Sensitivity of the normalised aggregated inertia and damping constants to different limits applied to the frequency security metrics.

5.4 Scalability

The proposed algorithms are further tested on a 30-bus MV distribution network with the planning solutions and frequency support presented in Table 5 considering four representative days. Both A1 and A2 outperform A0 in terms of total planning costs. It is observed that while A1 and A2 still indicate identical investment decisions, the former indicates a lower total cost due to low operational costs. The selection between algorithms A1 and A2 ultimately hinges on which provides computational efficiency and the optimality of the final solution. The results in Table 5 further indicate the optimal solution of the 30-bus network with varying RoCoF limits. It can be seen that the CIG with VSM-based CIG , PV_1, is adopted when more interia is required in the network due to the more restrictive security constraints.

5.5 Computational Performance

The computation performance for the different algorithms under study is presented in Fig. 7 considering cases with normal and tighter limits. Compared to A1 and A2, algorithm A0 consistently requires longer computational times to solve all case studies. Using A1 or A2 results in an average 25% reduction in computational time. The dual-cutting planes generated by the A1 and A2 more effectively eliminate infeasible problem spaces, leading to faster convergence compared to the approach in A0, which solely limits power exchange with the main grid.

Figure 7 further presents results for both the 18-bus and 30-bus networks indicating an increase in computational time with an increase in the size of the network and number of investment candidates as expected. For each study network, one of three CIGS types can be chosen as an investment candidate. However, the increase in the number of investment candidates further increases the investment decisions to be made. In the 30-bus network with seven investment

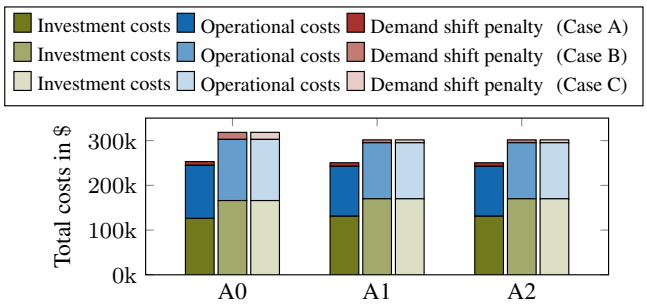

Fig. 6: Fluctuation of total costs with tighter security bounds for Case B (Tightening RoCoF) and Case C (Tightening quasi-steady-state frequency deviation limit)

Table 5 Planning solutions for the 30-bus network with varying RoCoF limits.

(a) Case A: RoCoF limit = 2 Hz/s.

	Algorithm 0	**Algorithm 1**	**Algorithm 2**
Costs and decisions			
Total cost ($)	3045089	2881913	2960361
Investment decision	$2\times PV_3$, $2\times SG$	$2\times PV_2$, $2\times SG$	$2\times PV_2$, $2\times SG$
Frequency support			
M (s)	15.60	15.60	15.60
D (p.u)	1.17	34.50	34.50

(b) Case B: RoCoF limit = 1 Hz/s.

	Algorithm 0	**Algorithm 1**	**Algorithm 2**
Costs and decisions			
Total cost ($)	3760089	3131387	3140962
Investment decision	$2\times PV_3$, $1\times PV_3$, $2\times SG$	$1\times PV_1$, $1\times PV_3$, $2\times SG$	$1\times PV_1$, $1\times PV_3$, $2\times SG$
Frequency support			
M (s)	15.60	22.60	22.60
D (p.u)	17.84	1.47	1.47

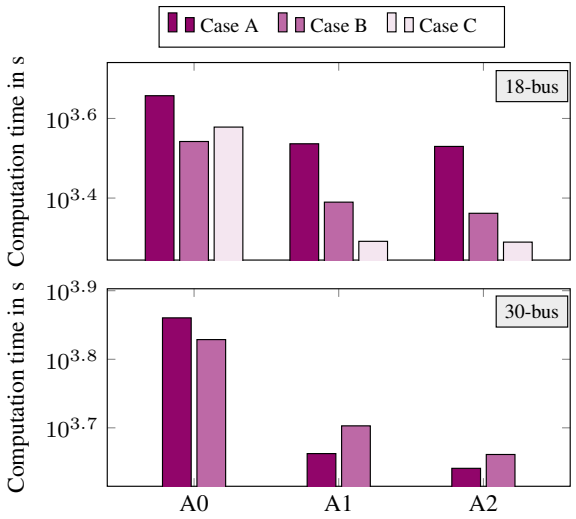

Fig. 7: Comparison of computational performance of the algorithms A0, A1 and A2, across Cases A, B and C for the 18-bus and 30-bus test networks.

candidates, there is a 60%, 34%, and 29% increase in the computation time for A0, A1, and A2, respectively, as compared to the 18-bus network with four investment candidates. This indicates that the proposed algorithms A1 and A2 scale better as the decision variables increase in number as opposed to A1. Moreover, imposing stricter security limits leads to a decrease in computational time for all networks. This is due to the reduced solution space resulting from the tighter constraints.

6 Conclusion

The abrupt disconnection of MGs from the main grid can trigger cascading failures caused by the activation of different protective devices in the network. It is therefore vital that the effect of these high-impact events is embedded in the planning model to ensure system security and resilience. However, most of the existing investment planning methods only consider the static pre- and post-fault security constraints while ignoring the transient security of the MG during the islanding event. In this paper, two tractable algorithms are proposed to provide a cost-effective transiently secure solution incorporating the frequency behaviour after islanding into the planning problem. The proposed algorithms adopt effective and efficient decomposition strategies to integrate non-linear transient frequency security constraints tractably. Moreover, the proposed solution algorithms concurrently optimise the required level of frequency support and system costs.

The methods presented in this work employed the CoI, which aggregates the contribution of each unit, to model the frequency trajectory during the transient state of the MG. However, with the increasing penetration of CIGs and distributed energy resources, greater variations in the local frequency response can be expected. Furthermore, the intermittent power generation of renewable resources can result in variations in the inertia support levels available in the network at a given time. Moreover, generating units located nearer to the location of the point of the fault, i.e., the MG point-of-common-coupling, may experience larger deviations as compared to those further away [50]. While the proposed methodologies are able to incorporate distributed frequency responses, further investigations are necessary to ensure model robustness and computational tractability with the increasing decision variables. Moreover, a distribution-free distributionally robust optimisation algorithm will be integrated to further tackle the uncertainties that can be experienced during system operation.

Author Contributions

Agnes Marjorie Nakiganda: Conceptualization, Formal analysis, Methodology, Writing – original draft, Writing – review and editing. **Shahab Dehghan**: Methodology, Writing – review and editing. **Petros Aristidou**: Funding acquisition, Methodology, Resources, Supervision, Writing – review and editing

Acknowledgements

This work was partially supported by the Engineering and Physical Sciences Research Council EPSRC) in the UK under grant reference EP/R030243/1.

Conflict of Interest Statement

The authors declare no conflicts of interest.

Data Availability Statement

The data that support the findings of this study are available from the corresponding author upon reasonable request.

7 References

1 J. Qiu, J. Zhao, F. Wen, J. Zhao, C. Gao, Y. Zhou, Y. Tao, and S. Lai, "Challenges and pathways of low-carbon oriented energy transition and power system planning strategy: a review," *IEEE Transactions on Network Science and Engineering*, pp. 1–21, 2023.

2 M. Panteli and P. Mancarella, "The grid: Stronger, bigger, smarter?: Presenting a conceptual framework of power system resilience," *IEEE Power and Energy Magazine*, vol. 13, no. 3, pp. 58–66, 2015.

3 M. Izadi, S. H. Hosseinian, S. Dehghan, A. Fakharian, and N. Amjady, "A critical review on definitions, indices, and uncertainty characterization in resiliency-oriented operation of power systems," *International Transactions on Electrical Energy Systems*, vol. 31, no. 1, p. e12680, 2021.

4 IEEE, "Ieee standard for the specification of microgrid controllers," *IEEE Std 2030.7-2017*, pp. 1–43, 2018.

5 A. H. Kasem Alaboudy, H. H. Zeineldin, and J. Kirtley, "Microgrid stability characterization subsequent to fault-triggered islanding incidents," *IEEE Trans. on Pow. Delivery*, vol. 27, no. 2, pp. 658–669, 2012.

6 M. Farrokhabadi, C. A. Cañizares, J. W. Simpson-Porco, E. Nasr, L. Fan, P. A. Mendoza-Araya, R. Tonkoski, U. Tamrakar, N. Hatziargyriou, D. Lagos, R. W. Wies, M. Paolone, M. Liserre, L. Meegahapola, M. Kabalan, A. H. Hajimiragha, D. Peralta, M. A. Elizondo, K. P. Schneider, F. K. Tuffner, and J. Reilly, "Microgrid stability definitions, analysis, and examples," *IEEE Transactions on Power Systems*, vol. 35, no. 1, pp. 13–29, 2020.

7 F. Milano, F. Dörfler, G. Hug, D. J. Hill, and G. Verbič, "Foundations and challenges of low-inertia systems (invited paper)," in *2018 Power Systems Computation Conference (PSCC)*, 2018, pp. 1–25.

8 W. Zheng, P. Crossley, B. Xu, and H. Qi, "Transient stability of a distribution subsystem during fault-initiated switching to islanded operation," *Int. Journal of Elec. Pow. & Energy Sys.*, vol. 97, pp. 418–427, 2018.

9 C. Gouveia, J. Moreira, C. L. Moreira, and J. A. Peças Lopes, "Coordinating storage and demand response for microgrid emergency operation," *IEEE Transactions on Smart Grid*, vol. 4, no. 4, pp. 1898–1908, 2013.

10 Y. Wu, G. J. Lim, and J. Shi, "Stability-constrained microgrid operation scheduling incorporating frequency control reserve," *IEEE Transactions on Smart Grid*, vol. 11, no. 2, pp. 1007–1017, 2020.

11 A. Khodaei, "Microgrid optimal scheduling with multi-period islanding constraints," *IEEE Transactions on Power Systems*, vol. 29, no. 3, pp. 1383–1392, 2014.

12 S. Karagiannopoulos, J. Gallmann, M. G. Vayá, P. Aristidou, and G. Hug, "Active distribution grids offering ancillary services in islanded and grid-connected mode," *IEEE Transactions on Smart Grid*, vol. 11, no. 1, pp. 623–633, 2020.

13 P. M. Anderson and M. Mirheydar, "A low-order system frequency response model," *IEEE Trans. Power Syst.*, vol. 5, no. 3, pp. 720–729, Aug 1990.

14 Kundur, P, Neal J. Balu, and Mark G. Lauby, *Power system stability and control*. New York: McGraw-Hill, 1994.

15 U. Markovic, Z. Chu, P. Aristidou, and G. Hug, "LQR-Based Adaptive Virtual Synchronous Machine for Power Systems with High Inverter Penetration," *IEEE Trans. Sustain. Energy*, vol. 10, no. 3, pp. 1501–1512, July 2019.

16 F. Teng, V. Trovato, and G. Strbac, "Stochastic scheduling with inertia-dependent fast frequency response requirements," *IEEE Transactions on Power Systems*, vol. 31, no. 2, pp. 1557–1566, 2016.

17 L. Badesa, F. Teng, and G. Strbac, "Simultaneous scheduling of multiple frequency services in stochastic unit commitment," *IEEE Transactions on Power Systems*, vol. 34, no. 5, pp. 3858–3868, 2019.

18 Z. Zhang, E. Du, F. Teng, N. Zhang, and C. Kang, "Modeling frequency dynamics in unit commitment with a high share of renewable energy," *IEEE Transactions on Power Systems*, vol. 35, no. 6, pp. 4383–4395, 2020.

19 M. Paturet, U. Markovic, S. Delikaraoglou, E. Vrettos, P. Aristidou, and G. Hug, "Stochastic unit commitment in low-inertia grids," *IEEE Trans. Power Syst.*, pp. 1–1, 2020.

20 Z. Zhang, M. Zhou, Z. Wu, S. Liu, Z. Guo, and G. Li, "A frequency security constrained scheduling approach considering wind farm providing frequency support and reserve," *IEEE Transactions on Sustainable Energy*, vol. 13, no. 2, pp. 1086–1100, 2022.

21 Y. Shen, W. Wu, B. Wang, and S. Sun, "Optimal allocation of virtual inertia and droop control for renewable energy in stochastic look-ahead power dispatch," *IEEE Transactions on Sustainable Energy*, vol. 14, no. 3, pp. 1881–1894, 2023.

22 Z. Chu, G. Cui, and F. Teng, "Scheduling of software-defined microgrids for optimal frequency regulation," *IEEE Transactions on Sustainable Energy*, vol. 15, no. 3, pp. 1715–1728, 2024.

23 Y. Zhang, C. Chen, G. Liu, T. Hong, and F. Qiu, "Approximating trajectory constraints with machine learning – microgrid islanding with frequency constraints," *IEEE Transactions on Power Systems*, vol. 36, no. 2, pp. 1239–1249, 2021.

24 Y. Shen, W. Wu, B. Wang, Y. Yang, and Y. Lin, "Data-driven convexification for frequency nadir constraint of unit commitment," *Journal of Modern Power Systems and Clean Energy*, vol. 11, no. 5, pp. 1711–1717, 2023.

25 A. M. Nakiganda, S. Dehghan, U. Markovic, G. Hug, and P. Aristidou, "A stochastic-robust approach for resilient microgrid investment planning under static and transient islanding security constraints," *IEEE Transactions on Smart Grid*, pp. 1–1, 2022.

26 S. Dehghan, N. Amjady, and P. Aristidou, "A robust coordinated expansion planning model for wind farm-integrated power systems with flexibility sources using affine policies," *IEEE Systems Journal*, 2019.

27 M. Farivar and S. H. Low, "Branch flow model: Relaxations and convexification—part i," *IEEE Trans. on Power Sys.*, vol. 28, no. 3, pp. 2554–2564, 2013.

28 A. M. Nakiganda, S. Dehghan, and P. Aristidou, "Comparison of AC optimal power flow methods in low-voltage distribution networks," in *2021 IEEE PES Innovative Smart Grid Technologies Europe (ISGT Europe)*. IEEE, 2021, pp. 1–5.

29 J. Rocabert, A. Luna, F. Blaabjerg, and P. Rodríguez, "Control of power converters in AC microgrids," *IEEE Trans. Power Electron.*, vol. 27, no. 11, pp. 4734–4749, Nov 2012.

30 U. Markovic, O. Stanojev, P. Aristidou, and G. Hug, "Partial grid forming concept for 100% inverter-based transmission systems," in *2018 IEEE PES GM*, 2018, pp. 1–5.

31 A. Ortega and F. Milano, "Impact of frequency estimation for vsc-based devices with primary frequency control," in *2017 IEEE PES Innovative Smart Grid Technologies Conference Europe (ISGT-Europe)*, 2017, pp. 1–6.

32 U. Markovic, O. Stanojev, P. Aristidou, E. Vrettos, D. Callaway, and G. Hug, "Understanding small-signal stability of low-inertia systems," *IEEE Transactions on Power Systems*, vol. 36, no. 5, pp. 3997–4017, 2021.

33 European Commission, "Commission regulation (EU) 2016/631 of 14 april 2016 establishing a network code on requirements for grid connection of generators (RfG)," *Official Journal of the European Union*, 2016.

34 U. Markovic, V. Häberle, D. Shchetinin, G. Hug, D. Callaway, and E. Vrettos, "Optimal sizing and tuning of storage capacity for fast frequency control in low-inertia systems," in *2019 International Conference on Smart Energy Systems and Technologies (SEST)*, 2019, pp. 1–6.

35 Y. Wen, W. Li, G. Huang, and X. Liu, "Frequency dynamics constrained unit commitment with battery energy storage," *IEEE Transactions on Power Systems*, vol. 31, no. 6, pp. 5115–5125, 2016.

36 P. Belotti, C. Kirches, S. Leyffer, J. Linderoth, J. Luedtke, and A. Mahajan, "Mixed-integer nonlinear optimization," *Acta Numerica*, vol. 22, p. 1–131, 2013.

37 A. J. Conejo, E. Castillo, R. Minguez, and R. Garcia-Bertrand, *Decomposition techniques in mathematical programming: engineering and science applications*. Springer Science & Business Media, 2006.

38 E. Kägi-Kolisnyc, "Distribution Management System Including Dispersed Generation and Storage in a Liberalized Market Environment," Ph.D. dissertation, EPFL, Lausanne, Switzerland, 01 2009.

39 A. M. Nakiganda and P. Aristidou, "Resilient microgrid scheduling with secure frequency and voltage transient response," *IEEE Transactions on Power Systems*, vol. 38, no. 4, pp. 3580–3592, 2023.

40 A. Khodaei, S. Bahramirad, and M. Shahidehpour, "Microgrid planning under uncertainty," *IEEE Transactions on Power Systems*, vol. 30, no. 5, pp. 2417–2425, 2015.

41 U.S. Energy Information Administration, "Levelized costs of new generation resources in the annual energy outlook 2022," 2022. [Online]. Available: https://www.eia.gov/outlooks/aeo/pdf/electricity_generation.pdf

42 J. Löfberg, "Yalmip : A toolbox for modeling and optimization in matlab," in *2004 IEEE Intern. Conf. on Robotics and Automation*, 2004, pp. 284–289.

43 Gurobi Optimization, LLC, "Gurobi optimizer reference manual," 2020. [Online]. Available: http://www.gurobi.com

44 X. Wu, Z. Wang, T. Ding, X. Wang, Z. Li, and F. Li, "Microgrid planning considering the resilience against contingencies," *IET Generation, Transmission Distribution*, vol. 13, no. 16, pp. 3534–3548, 2019.

45 E. Yamangil, R. Bent, and S. Backhaus, "Resilient upgrade of electrical distribution grids," in *29th AAAI Conf. on Artificial Intelligence*, 2015.

46 Y. Lin and Z. Bie, "Tri-level optimal hardening plan for a resilient distribution system considering reconfiguration and dg islanding," *Applied Energy*, vol. 210, pp. 1266 – 1279, 2018.

47 W. Yuan, J. Wang, F. Qiu, C. Chen, C. Kang, and B. Zeng, "Robust optimization-based resilient distribution network planning against natural disasters," *IEEE Trans. Smart Grid*, vol. 7, no. 6, pp. 2817–2826, 2016.

48 M. Sengupta, Y. Xie, A. Lopez, A. Habte, G. Maclaurin, and J. Shelby, "The national solar radiation data base (nsrdb)," *Renewable and Sustainable Energy Reviews*, vol. 89, pp. 51–60, 2018.

49 P. Aristidou, S. Lebeau, and T. Van Cutsem, "Power system dynamic simulations using a parallel two-level schur-complement decomposition," *IEEE Trans. on Power Sys.*, vol. 31, no. 5, pp. 3984–3995, 2016.

50 F. Milano and A. Ortega, "Frequency divider," *IEEE Transactions on Power Systems*, vol. 32, no. 2, pp. 1493–1501, 2017.